

# Lightweight soft neuroprosthetic hand

**Guoying Gu**

Shanghai Jiao Tong University <https://orcid.org/0000-0002-7778-4523>

**Ningbin Zhang**

Shanghai Jiaotong University

**Haipeng Xu**

Shanghai Jiaotong University

**Shaoting Lin**

MIT

**Yang Yu**

Shanghai Jiaotong University <https://orcid.org/0000-0001-5582-4558>

**Guohong Chai**

Shanghai Jiaotong University <https://orcid.org/0000-0002-5756-6887>

**Lisen Ge**

Shanghai Jiaotong University

**Houle Yang**

Shanghai Jiaotong University

**Qiwen Shao**

Shanghai Jiao Tong University

**Xinjun Sheng**

Shanghai Jiaotong University

**Xiangyang Zhu**

Shanghai Jiaotong University

**Xuanhe Zhao** (✉ [zhaox@mit.edu](mailto:zhaox@mit.edu))

Massachusetts Institute of Technology <https://orcid.org/0000-0001-5387-6186>

---

## Article

### Keywords:

**Posted Date:** August 10th, 2020

**DOI:** <https://doi.org/10.21203/rs.3.rs-47149/v1>

**License:**   This work is licensed under a Creative Commons Attribution 4.0 International License.

[Read Full License](#)

---

**Version of Record:** A version of this preprint was published at Nature Biomedical Engineering on August 16th, 2021. See the published version at <https://doi.org/10.1038/s41551-021-00767-0>.

## Lightweight soft neuroprosthetic hand

Guoying Gu<sup>1,2†\*</sup>, Ningbin Zhang<sup>1†</sup>, Haipeng Xu<sup>1</sup>, Shaoting Lin<sup>3</sup>, Yang Yu<sup>1</sup>, Guohong Chai<sup>1</sup>, Lisen Ge<sup>1</sup>, Houle Yang<sup>1</sup>, Qiwen Shao<sup>1</sup>, Xinjun Sheng<sup>1,2</sup>, Xiangyang Zhu<sup>1,2†\*</sup>, and Xuanhe Zhao<sup>3,4†\*</sup>

<sup>1</sup>Robotics Institute, School of Mechanical Engineering, Shanghai Jiao Tong University, Shanghai 200240, China; <sup>2</sup>State Key Laboratory of Mechanical System and Vibration, Shanghai Jiao Tong University, Shanghai 200240, China; <sup>3</sup>Department of Mechanical Engineering, Massachusetts Institute of Technology, Cambridge, MA 02139, USA; <sup>4</sup>Department of Civil and Environmental Engineering, Massachusetts Institute of Technology, Cambridge, MA 02139, USA

†These authors contributed equally to the current work.

\*Authors to whom correspondence should be addressed: [zhaox@mit.edu](mailto:zhaox@mit.edu), [guguoying@sjtu.edu.cn](mailto:guguoying@sjtu.edu.cn), [mexyzhu@sjtu.edu.cn](mailto:mexyzhu@sjtu.edu.cn)

### Abstract

Mainly composed of electrical motors and sophisticated mechanical components, existing neuroprosthetic hands<sup>1,2</sup> are typically heavy (>400 g) and expensive (>USD 10,000), and they lack the compliance and tactile feedback of human hands. These limitations hamper neuroprosthetic hands' innovation and broad utility for amputees<sup>3-5</sup>. Here we report the design, fabrication and applications of a lightweight (292 g) and potentially low-cost (component cost below USD 500) soft neuroprosthetic hand with simultaneous myoelectric control and tactile feedback. The soft neuroprosthetic hand consists of five soft fingers and a palm to give six active degrees of freedom under pneumatic actuation, four electromyography sensors that measure the surface electromyogram signals to control the hand to deliver four common grasp types, and five hydrogel-elastomer capacitive sensors on the fingertips that measure the touch pressure and elicit electrical stimulation on the skin of the residual limb. The soft finger is made of a fiber-reinforced elastomeric structure embedded with rigid segments to mimic the soft-joint/rigid-bone anatomy of the human finger. We use a set of standardized tests<sup>6</sup> to compare the speed and dexterity of the soft neuroprosthetic hand and a conventional rigid neuroprosthetic hand<sup>7</sup> on two transradial amputees. The soft neuroprosthetic hand gives overall superior performances to the rigid hand. We further demonstrate that one transradial amputee wearing the soft neuroprosthetic hand can regain the versatile hand functions with primitive touch sensation and real-time closed-loop control in daily activities such as handling tools, eating, shaking hands, petting animals, and recognizing touch pressure. This work not only represents a new paradigm for designing soft

neuroprosthetic devices but also opens an avenue to widespread applications of **lightweight, low-cost, and compliant hand replacements for amputees.**

## **Introduction**

There are over five million upper-limb amputees worldwide, and the number increases by a substantial margin each year. Losing a hand is generally catastrophic, seriously limiting a person's ability in daily activities<sup>1</sup>. Although artificial prostheses are available, the most widely used prostheses are still cosmetic devices or functional hook-like grippers. While a few anthropomorphic neuroprosthetic hands<sup>1,2</sup> (such as i-Limb Hand, Michelangelo Hand, Bebionic Hand, and Vincent Hand) have been commercialized, they all rely on electrical motors and sophisticated mechanical components. The high weights (>400 g) and high prices (>USD 10,000) of these neuroprosthetic hands severely limit their broad utility for amputees<sup>3,4</sup>. It is also desirable for neuroprosthetic hands to have the compliance and tactile feedback of human hands<sup>1,2,5</sup>. **For instance, the Pisa/IIT SoftHand<sup>8-10</sup> composed of electrical motors and tendon-driven mechanisms with compliant joints or skins has been developed as a myoelectric prosthesis with high compliance and 520 g of weight. In addition, several recent studies<sup>11-18</sup> have been reported to investigate the invasive or noninvasive sensory feedback for upper-limb amputees, but they are only implemented in rigid neuroprosthetic hands.** The emerging field of soft robotics<sup>19-21</sup> that combines the compliance of human skin and muscle with simple design and fabrication of **lightweight** elastomeric components may open a promising avenue for future neuroprosthetic hands. Although many bioinspired soft robotic systems such as locomotive robots<sup>22</sup>, finger-like actuators<sup>23-26</sup>, robotic exoskeletons<sup>27-29</sup> and hands<sup>30-34</sup> have been developed, to the best of our knowledge, none of them has been demonstrated as functional neuroprosthetic hands on upper-limb amputees (Extended Data **Table 1**).

Here, we report the design, fabrication and applications of a lightweight (292 g) and potentially low-cost (component cost below USD 500) soft neuroprosthetic hand with simultaneous myoelectric control and tactile feedback for transradial amputees (**Fig. 1A** and Extended Data **Tables 2, 3**). The soft neuroprosthetic hand consists of five soft fingers and a palm to give six active degrees of freedom (DoFs), four electromyography sensors that measure the surface electromyogram (EMG) signals of residual forearm muscles to control the hand to deliver four common grasp types, and five hydrogel-elastomer capacitive sensors on the fingertips that measure touch pressure and elicit electrical stimulation on the skin of the residual limb. To evaluate the function of the soft neuroprosthetic hand, two transradial amputees have carried out a set of standardized tests<sup>6</sup> (including the Box and Blocks Test, all seven tasks in the Jebsen-Taylor Hand Function Test, and nine selected tasks in the Southampton Hand Assessment Procedure). One transradial amputee with the soft neuroprosthetic hand has further demonstrated the dexterous and versatile hand functions with primitive tactile sensation and closed-loop control in daily activities such as handling tools, eating, shaking hands, petting animals, and recognizing touch pressure.

## **Design**

*Hand.* Each finger of the soft neuroprosthetic hand is based on a fiber-reinforced elastomeric tubular structure, in which two or three rigid segments with specific lengths are embedded to mimic the soft-joint/rigid-bone anatomy of the thumb or other fingers, respectively, of a human hand<sup>35,36</sup> (**Fig. 1B** and Supplementary **Figs. 1, 2**). The thumb-palm connection in the soft neuroprosthetic hand is based on a fiber-reinforced elastomeric hollow pad with a strain-limiting layer (Supplementary **Fig. 3**). The soft neuroprosthetic hand is designed to possess six active DoFs (**Fig. 1C**): each soft finger can be pneumatically actuated to provide one flexion DoF and the thumb-palm

connection under pneumatic actuation further gives the thumb another circumduction DoF. In addition, the inherent compliance of the soft fingers can introduce many passive DoFs to the soft hand for dexterous and adaptive grasps even on fragile and soft objects (**Fig. 1D**), mimicking those passive compliance of human hands<sup>8</sup>.

We choose the pneumatically-actuated soft fingers owing to their advantages of low cost, light weight, and scalable fabrication<sup>21</sup>. As the applied pneumatic pressure to a soft finger increases, the bending angles of the flexible joints increase. We develop an analytical model to study the bending angles of a soft finger's flexible joints (see Methods section "Analytical model for the design of the soft finger"). The model demonstrates that, with a fixed finger length, the bending angles of the flexible joints are linearly proportional to the lengths of the flexible joints. This trend is consistent with the experimental results (Supplementary **Figs. 4, 5**). We further develop a finite-element model to quantitatively predict the bending angles of the flexible joints and the deformation of the soft finger upon pneumatic actuation (see Methods section "Finite-element model for the design of the soft finger"). The finite-element model is in quantitative agreement with the experimental results (**Fig. 1E**, Extended Data **Fig. 1** and Supplementary **Video 1**). For example, the finite-element model predicts that the three flexible joints in the soft index finger under the maximum pneumatic actuation of 120 kPa give the bending angles of 84.02°, 112.58° and 52.55°, only deviating from the experimental results by 3.25%, 11.60% and 7.44%, respectively (Extended Data **Table 4**).

The five soft fingers are mounted on a three-dimensionally (3D) printed plastic palm (Imagine 8000, SOMOS Inc., Netherlands) in the shape of a human palm. Both the fingers and the palm are covered by a soft elastomeric layer mimicking the skin on the human hand. The palm skeleton is further connected to a customized plastic socket that fits with the residual limb of the transradial amputee. Owing to the pneumatic actuation and modular design of the soft neuroprosthetic hand,

the pumps, valves, electronic boards and battery for the hand can be contained in a small bag (total weight of 444 g) on the waist of the amputee (Extended Data **Fig. 2A**). The pumps and electronic board are connected by soft tubing and electrical wires (hidden under clothes and in the socket) to the soft fingers and sensors on the hand, respectively. This modular design can dramatically reduce the weight of the soft neuroprosthetic hand to 292 g, much lighter than the weights of commercially-available neuroprosthetic hands (420 g - 628 g; Extended Data **Table 3**) and the average human hands (400 g)<sup>1,2</sup>. Furthermore, since the commercially-available neuroprosthetic hands integrate the electric motors, transmission mechanisms and batteries in their palms and sockets, it is challenging to significantly reduce their weights. We further demonstrate that the six active DoFs of the soft neuroprosthetic hand can be independently controlled with one pump and twelve valves (Supplementary **Video 2**). Notably we can also integrate the pumps, valves, electronic boards and battery in the socket of the soft neuroprosthetic hand if required in any application (Extended Data **Fig. 2B**). Such a design increases the weight of the soft neuroprosthetic hand to 604 g, which is still lighter than or comparable to the weights of commercially-available neuroprosthetic hands such as the i-Limb large hand and the Bebionic medium hand (Extended Data **Table 3**).

*EMG sensors.* In the socket of the hand, we implement four customized EMG sensors (**Fig. 1A** and Extended Data **Fig. 3**), which will be mounted on the skin of the residual limb to record the surface EMG signals from the target muscles in the residual limb. Each EMG sensor (weight of 10 g) consists of three electrodes (a reference electrode and a pair of differential electrodes) and readout electronics (including two-level signal amplifier and filter circuits; see Supplementary **Fig. 6**). The locations of the EMG sensors with respect to the target muscles have been optimized, aiming to achieve a superior performance on decoding the amputees' motion intention. The decoded motion intention will be used to control the soft fingers and palm to deliver the corresponding grasp types.

*Touch sensors and electrical stimulators.* To sense the touch pressure of the soft neuroprosthetic hand applying on objects, we implement five soft capacitive touch sensors, each on a fingertip of the hand (**Fig. 1C**). The capacitive touch sensor is composed of an ionic hydrogel-elastomer hybrid structure<sup>37-39</sup> that forms a capacitor for sensing the touch pressure (Supplementary **Fig. 7A**). An increase in the touch pressure reduces the thickness of the elastomeric layer and, therefore, increases the capacitance of the capacitor (Supplementary **Fig. 7B**). The measured relative capacitance change is used to control an electrical stimulator (Supplementary **Fig. 8**), which outputs programmable electrical pulses via a noninvasive stimulation electrode on a specific region of the residual limb (Supplementary **Fig. 9**) to inform the amputee the touch pressure on the corresponding fingertip. This is the first time that hydrogel-elastomer capacitive touch sensors have been used on the soft neuroprosthetic hand to measure the touch pressure at the fingertips.

*Control algorithm.* By integrating the EMG sensors, touch sensors and electrical stimulators with the hand, we develop a bidirectional human-machine interface for the soft neuroprosthetic hand (Supplementary **Fig. 8** for the description of experimental setup). We choose a pattern recognition approach<sup>40</sup> to classify the surface EMG signals into five classes corresponding to the four common grasp types<sup>41,42</sup> and rest type of human hands (see Supplementary Information for the descriptions of pattern recognition algorithms). The decoded grasp types are then mapped onto the actuation command for the corresponding soft fingers and palm. Based on the relative changes of the measured capacitances of the capacitive touch sensors (caused by the touch pressure), we can program the electrical stimulator to output the corresponding stimulation patterns, which inform the amputee the touch pressure on each fingertip. Based on the informed touch pressure, the amputee can further change the grasp type of the soft neuroprosthetic hand by varying the EMG signals, therefore forming a closed-loop control of the hand.



## Characterization

We use a simple and scalable method to fabricate and assemble the soft neuroprosthetic hand (see Methods section “Fabrication and assembly of the soft neuroprosthetic hand” and Extended Data **Fig. 4**). We next characterize the performance of the fabricated soft neuroprosthetic hand. To monitor its kinematics, we develop a motion tracking system (Supplementary **Fig. 10**). For the 1-DoF flexion fingers (i.e., index, middle, ring, and little fingers), we attach markers to their flexible joints and fingertips to measure the bending angles of the joints and the fingertips (**Fig. 2A**). We find that an increase of the applied pneumatic pressure increases the bending angles of the fingertip to a maximum of  $231^\circ$  at 120 kPa pneumatic pressure (**Fig. 2B**). In addition, the measured bending angles of the flexible joints are consistent with the finite-element model’s prediction (**Fig. 2B**, Extended Data **Fig. 1A** and Extended Data **Table 4**). For the 2-DoF thumb, we attach markers to its flexible joints, thumb tip and thumb-palm connection (**Fig. 2C**). The results indicate that the thumb has a maximum flexion of  $69^\circ$  and a maximum palm circumduction of  $28^\circ$  at 80 kPa pneumatic pressure, which also agrees well with the finite-element model’s prediction (**Fig. 2D**, Extended Data **Fig. 1B**, Supplementary **Fig. 11** and Extended Data **Table 4**). The maximum bending angles of the soft fingers are comparable to those of existing rigid counterparts (Extended Data **Table 3**).

To evaluate the load capacity of the soft neuroprosthetic hand, we use the hand (at 100 kPa pneumatic pressure to the 1-DoF fingers and 80 kPa pneumatic pressure to the 2-DoF thumb) to grasp a 55 mm-diameter cylinder while measuring the grasping force with an electronic dynamometer (Supplementary **Fig. 12**). The results indicate that the soft neuroprosthetic hand gives maximum grasping forces of 18 N and 17 N along the vertical and horizontal directions, respectively

(**Fig. 2E, F**). Therefore, the soft neuroprosthetic hand can perform most grasping tasks in daily activities, which generally require grasping forces below 10 N for human hands<sup>43</sup>. The grasping forces of the soft fingers can be potentially increased in future studies by using stiffer elastomers for the fingers and applying higher pneumatic pressures.

Furthermore, we demonstrate that our soft fingers have repeatable pressure-flexion relations with small hysteresis over 10,000 cycles of actuations (**Fig. 2G**), and they are resilient to be bent by arbitrary angles, struck with a steel hammer, and run over back and forth by one wheel of a 1500 kg vehicle (Supplementary **Fig. 13** and Supplementary **Video 3**).

Based on the usage frequencies of grasp types in daily activities<sup>41,42</sup>, we choose to recognize the most commonly used four grasp types (i.e., Power, Precision disk, Tripod and Lateral pinch) of amputees through the myoelectric control interface (Extended Data **Fig. 5**). Using the four-channel EMG sensors (one sensor at each channel), the soft neuroprosthetic hand can decode the intended four grasp types and rest type (**Fig. 2H** and Supplementary **Fig. 14**).

We next calibrate the capacitive touch sensor by uniformly compressing the sensor and then measuring its capacitance. Under zero pressure, we denote the measured capacitance of the sensor as  $C_0$ . With the increase of the applied pressure, we can obtain the current capacitance  $C$  of the touch sensor and calculate the change of the capacitance  $\Delta C = C - C_0$ . The experimental results demonstrate that, when the uniformly applied pressure on the sensor increases from 0 kPa to 55.8 kPa, the  $\Delta C/C_0$  varies from 0 to 0.85, giving a sensitivity of  $0.016 \text{ kPa}^{-1}$  (Supplementary **Fig. 7B**).

## **Applications on amputees**

*Performances of soft and rigid neuroprosthetic hands.* The soft neuroprosthetic hand can restore the versatile hand functions for amputees. A subject with transradial amputation can adapt

to the soft neuroprosthetic hand and master its functions after training for 15 minutes (Extended Data **Fig. 6** and Supplementary **Video 4**). We use a set of standardized tests<sup>6</sup> to evaluate the performances of the soft neuroprosthetic hand (**Fig. 3A**, Extended Data **Fig. 7**, and Supplementary **Video 5**), including the Box and Blocks Test (BBT, i.e., counting the number of blocks that can be grasped and transported per minute), all seven tasks in the Jebsen-Taylor Hand Function Test (i.e., J1-writing, J2-simulated page-turning, J3-lifting small common objects, J4-simulated feeding, J5-stacking checkers, J6-lifting large light objects, and J7-lifting large heavy objects), and nine selected tasks in the Southampton Hand Assessment Procedure (i.e., grasping nine kinds of objects including S1-spherical light, S2-spherical heavy, S3-tripod light, S4-power light, S5-power heavy, S6-tip light, S7-tip heavy, S8-extension light, and S9-extension heavy). As a comparison, the same subject wearing a conventional rigid neuroprosthetic hand<sup>7</sup> trained by the same amount of time (about 15 minutes) has performed the same set of standardized tests (Supplementary **Fig. 15** and Supplementary **Video 6**). Throughout the tests, the subject feels that the soft neuroprosthetic hand is much lighter to wear than the rigid neuroprosthetic hand. **Statistical analyses (Fig. 3A and Extended Data Table 5)** further demonstrate that, compared to the rigid neuroprosthetic hand, the soft neuroprosthetic hand has significantly superior performances in 7 items (i.e., BBT, J3, J4, J7, S1, S3 and S5), significantly inferior performances in 3 items (i.e., J5, S6 and S7), and statistically similar performances ( $p > 0.05$ ) in 7 items (i.e., J1, J2, J6, S2, S4, S8 and S9). Based on the same set of standardized tests and statistical analyses (Extended **Data Fig. 8** and Extended Data **Table 6**), another subject with transradial amputation demonstrates that the performances of the soft neuroprosthetic hand are significantly superior in 5 items (i.e., J3, J5, S4, S5 and S8), significantly inferior in 4 items (i.e., J1, S6, S7 and S9), and statistically similar in 8 items (i.e., BBT, J2, J4, J6, J7, S1, S2 and S3) compared to those of the rigid counterpart (Supplementary **Fig. 16**)<sup>45-47</sup>. (Note

the reported results have only provided mean values of their performances, whose statistical difference from the performances of the soft neuroprosthetic hand cannot be evaluated.)

Next, we perform comparative experiments for the same subject wearing the soft neuroprosthetic hand and the rigid i-Limb hand to grasp fragile objects (e.g., strawberry, bread, paper cup). The results indicate that the rigid neuroprosthetic hand damages the strawberry and bread, and tends to crush the paper cup (Extended Data **Fig. 9A** and Supplementary **Video 7**). Owing to the inherent compliance, the soft neuroprosthetic hand can guarantee safe interactions with these fragile and soft objects (Extended Data **Fig. 9B** and Supplementary **Video 7**).

Furthermore, we demonstrate that one subject with the soft neuroprosthetic hand can intuitively perform the four common grasp types to grasp different objects (Supplementary **Video 8**) and handle commonly-used items in daily activities, such as food (e.g., potato chips, cakes, strawberries and apples), commodities (e.g., clothes, bags, laptops, water glasses, bottles, tissues and dishes), and tools (e.g., hammers and pliers). The subject also achieves safe interactions with other persons (e.g., shaking hands), animals (e.g., petting a cat) and environments (e.g., touching a flower) (**Fig. 3B** and Supplementary **Video 9**). We further demonstrate that the subject can successfully carry out delicate tasks to handle objects with complex shapes and different sizes and then insert them in the corresponding slots precisely (**Fig. 3C**, and Supplementary **Video 10**). In a load test, the subject wearing the soft neuroprosthetic hand can lift a payload of 2.3 kg (**Fig. 3D** and Supplementary **Video 11**).

*Tactile feedback and closed-loop control.* Furthermore, we demonstrate that the subject with the soft neuroprosthetic hand can restore primitive touch sensation based on the capacitive touch sensors and electrical stimulators. When the effective pressure on the touch sensor of a fingertip reaches a threshold (i.e., threshold  $\Delta C/C_0$ ), the electrical stimulator will be triggered to generate an

electrical pulse (amplitude of 4.0 mA, pulse width of 200  $\mu$ s, and pulse frequency of 20 Hz) to stimulate a specific region on the residual limb corresponding to the fingertip (**Fig. 4A** and Supplementary **Fig. 9**). We set the threshold effective pressure to be 2.3 kPa (i.e., the threshold  $\Delta C/C_0 = 0.1$ ), so that the touch sensors are sufficiently sensitive to touch pressures commonly experienced in daily activities<sup>44</sup> yet unaffected by environmental noises and crosstalk among sensors (Supplementary **Fig. 17**). In a blindfolded and acoustically-shielded interaction experiment, we gently compress the five fingers of the soft neuroprosthetic hand in random combinations. The subject can almost instantaneously distinguish any individual finger or multiple fingers being compressed (**Fig. 4B** and Supplementary **Video 12**).

Next, we demonstrate the closed-loop control capability of the soft neuroprosthetic hand enabled by integrating the myoelectric control and the tactile feedback. In a blindfolded and acoustically-shielded experiment, the subject uses his own EMG signals to control the soft neuroprosthetic hand to give the power grasp type. If the hand firmly grasps a bottle so that the effective pressures on the five fingertips are above the threshold, the subject is informed by the electrical stimulators to lift up the bottle (**Fig. 4 C, D** and Supplementary **Video 13**). In contrast, if the hand does not grasp anything that applies pressure on the fingertips, the subject does not lift up but relaxes the hand after a few seconds (**Fig. 4 C, D** and Supplementary **Video 13**).

Furthermore, by programing the frequencies (i.e., 5 Hz, 20 Hz or 35 Hz) of the electrical pulses to map different ranges of  $\Delta C/C_0$  of the touch sensor on the middle finger (i.e., no stimulation when  $\Delta C/C_0 \leq 0.1$ , 5 Hz when  $0.1 < \Delta C/C_0 \leq 0.3$ , 20 Hz when  $0.3 < \Delta C/C_0 \leq 0.4$ , and 35 Hz when  $\Delta C/C_0 > 0.4$ ), we demonstrate that, in the blindfolded and acoustically-shielded experiment, the subject can restore the graded tactile feedback to discriminate three cylinders with different

diameters (i.e., 60 mm, 70 mm and 80 mm) with an accuracy of 96.25% (Extended Data **Fig. 10** and Supplementary **Video 14**).

## **Conclusion**

We report a lightweight and potentially low-cost soft neuroprosthetic hand for transradial amputees to restore versatile hand functions and primitive tactile sensation. We choose a modular design to enable efficient iteration of the design, fabrication and control, as well as rapid replacement of the components in case of wear or damage. Compared to commercially-available neuroprosthetic hands, our soft neuroprosthetic hand has advantages including the intrinsic compliance, light-weight (292 g), potentially low-cost (component cost below USD 500), and embedded soft touch sensors, while maintaining the similar active DoFs, the number of joints, and the maximum bending angles of the joints (Extended Data **Table 3**). As the first demonstration of the soft neuroprosthetic hand on transradial amputees, we employ the most commonly used EMG-decoding algorithm and the electrotactile feedback. To further improve the performance of the soft neuroprosthetic hand, advanced EMG-decoding algorithms<sup>48-50</sup> and sensory feedback approaches<sup>11-18</sup> can be implemented in the future. Overall, this work has the potential to provide the next-generation personalized neuroprosthetic hands that are intrinsically soft, lightweight and potentially low-cost for upper-limb amputees, and to broaden the future applications of soft robotic systems.

## Methods

### Synthesis of the ionic hydrogel

The ionic hydrogel<sup>37-39</sup> is a polyacrylamide (PAAm) hydrogel containing lithium chloride (LiCl). The PAAm-LiCl hydrogel is synthesized by using the acrylamide (AAM; J&K) as the monomer, N,N'-methylenebisacrylamide (MBAA; Molbase) as the crosslinker, LiCl monohydrate (LiCl·H<sub>2</sub>O; Sinopharm Chemical Reagent) as the ionic conductive medium, and 2-Ketoglutaric Acid (Adamas) as the photoinitiator. The monomer solution is prepared by mixing AAM, LiCl·H<sub>2</sub>O and deionized water with a mass ratio of 9.98%: 16.16%: 73.86%. MBAA solution is dissolved into deionized water with a mass ratio of 1.2%. Then, the monomer solution, MBAA solution, and 2-Ketoglutaric Acid are mixed with the mass ratio of 96.67%: 1.13%: 2.20% to form the hydrogel precursor ink for further fabrication. Note that the LiCl is added into the hydrogel, not only serving as a conductive medium but also as a hygroscopic salt to maintain water in the hydrogel in ambient environments<sup>37-39</sup>.

### Fabrication and assembly of the soft neuroprosthetic hand

We present a simple and scalable method to fabricate and assemble the soft neuroprosthetic hand (Extended Data Fig. 4). For the soft fingers, we use the Dragon Skin 10 (Smooth-On Inc., USA) silicone rubber for the inner elastomeric tubular structure, the Ecoflex 0030 (Smooth-On Inc., USA) silicone rubber for the outer elastomeric skin, and the polyethylene thread for the fiber reinforcement. We attach the carbon fiber-reinforced plastics lamination with the heat-shrink tubes as the embedded rigid segments of the soft fingers. The palm skeleton is 3D printed with the commercial photosensitive resin (Imagine 8000, SOMOS Inc., Netherlands) and the covered elastomeric skin is made of Ecoflex 0030 silicone rubber. To tune the color of the elastomeric skin close to the amputee's skin color, we can add Slic Pig pigment PMS 488C (Flesh color, Smooth on Inc., USA) into the Ecoflex 0030 silicone rubber (see Supplementary Fig. 18 for an illustration). The socket is fabricated with the vacuum-forming thermoplastic acrylic resin and the commercial gold-plated copper blocks are embedded in the socket as the EMG electrodes. We fabricate the capacitive touch sensors by curing the hydrogel precursor (containing acrylamide, crosslinker, photoinitiator, and ionic conductive medium) into a VHB elastomeric matrix. Notably, all the mechanical components can be constructed with low-cost commercially available materials (Extended Data Table 2). The fabrication and assembly steps of the soft neuroprosthetic hand are detailed in the Supplementary Information.

### Analytical model for the design of the soft finger

The method for efficiently predicting the bending angles of the flexible joints in the soft fingers plays an important role in mimicking the structure and function of human fingers<sup>24</sup>. We first develop an analytical model to analyze the pneumatic response of a flexible joint. We use a non-linear elasticity approach to analytically model the response of the flexible joint under pneumatic actuation. Specifically, we model the flexible joint as a hollow cuboid of isotropic incompressible neo-

Hookean solid with shear modulus of  $\mu$  and a stiff inextensible layer beneath the cuboid. We take the thickness, height, and width of the hollow cuboid at the undeformed state as  $t$ ,  $H$ , and  $W$ , respectively (Supplementary **Fig. 4A**). Due to the lateral constraint from the stiff fibers surrounding the cuboid, we assume the cross-sections of the cuboid remain planar upon pressurization, which has been validated by the finite-element simulation as well. Furthermore, since the arrangement of fibers are symmetric without twisting, we express the axial stretch of the cuboid cross-section in a linear form of  $\lambda_z(y) = y[\lambda_z(H) - 1]/H + 1$ , where  $\lambda_z(H) = \lambda_z^H = l/L$  is the axial stretch at the top surface with the elongated length of  $l$  at the top surface (Supplementary **Fig. 4A**). The deformation gradient at the side surfaces reduces to

$$\mathbf{F} = \begin{bmatrix} \lambda_z^{-1}(y) & 0 & 0 \\ 0 & 1 & 0 \\ 0 & 0 & \lambda_z(y) \end{bmatrix} \quad (1)$$

We model the elastomeric cuboid as an incompressible neo-Hookean solid with strain energy of  $W = \mu(\mathbf{FF}^T - 3)/2$ . Therefore, the axial nominal stress in the cuboid is

$$S_{zz}(y) = \mu \left[ \frac{y}{H}(\lambda_z^H - 1) + 1 \right] - \mu \left[ \frac{y}{H}(\lambda_z^H - 1) + 1 \right]^{-3} \quad (2)$$

Assuming the deformation of the hollow cuboid is pure bending, we can obtain the geometrical relation between the bending angle  $\alpha$  and the dimensions of the flexible joint (i.e.,  $l$ ,  $L$ , and  $H$ )

$$\alpha = \frac{l - L}{H} \quad (3)$$

Since the bending actuation is driven by the moment created by the internal pressure imposing on the cap of the flexible joint  $M_p$ , the relation between the pneumatic pressure  $p$  and the bending angle  $\alpha$  can be found by equating  $M_p$  to the moment generated by the internal stress of the elastomeric cuboid  $M_c$ . To calculate  $M_c$ , we take the stiff inextensible layer as the position of the neutral axis

$$M_c = 2 \int_0^H S_{zz}(y) y t dy + S_{zz}(H) W H t \quad (4)$$

The moment created by the internal pressure is

$$M_p = \int_0^H p W y dy \quad (5)$$

Solving Eq. (4) and Eq. (5) yields the relation between the pneumatic pressure and the bending angle as

$$\frac{2t}{3W} \left[ 2(\lambda_z^H)^3 - 3(\lambda_z^H)^2 + 6(\lambda_z^H)^{-1} - 3(\lambda_z^H)^{-2} - 2 \right] + \frac{2t}{H} \left[ (\lambda_z^H) - (\lambda_z^H)^{-3} \right] = \frac{p}{\mu} \quad (6a)$$

$$\lambda_z^H = \alpha \frac{H}{L} + 1 \quad (6b)$$

To verify the above analytical model, we further simulate the pneumatic response of the flexible joint, which consists of a cuboid elastomeric chamber, a network of stiff fibers surrounding the



elastomeric chamber, and a stiff layer beneath the chamber. We model the elastomeric chamber as a neo-Hookean solid with solid elements (C3D10H), the strain energy density of which is

$$W = \frac{\mu}{2}(\mathbf{FF}^T - 3) + \frac{\kappa}{2}(J - 1)^2 \quad (7)$$

where  $\mu$  is the shear modulus,  $\kappa$  is the bulk modulus,  $J = \det(\mathbf{F})$ . We set  $\mu=80$  kPa and  $\kappa/\mu = 1000$  to impose the nearly incompressibility of the material. The stiff layer is modeled as a skin of shell elements with Young's modulus of 210 GPa. The fiber is modeled as a beam element (B32H) with Young's modulus of 1 GPa. The fiber direction is set perpendicular to the axial direction of the finger to constrain the lateral expansion of the flexible joints during inflation<sup>17</sup>. Static simulations are performed by applying pressure on all internal faces of the elastomer chamber with zero displacements at the base portion of the finger as the boundary conditions. We first compare the axial stretch at the top surface of the flexible joint in experiments and simulations, verifying the main deformation mode of the flexible joints is the bending motion (Supplementary **Fig. 4B**). We further compare the increase of the bending angle  $\alpha$  as a function of the applied inflation pressure  $p$  for the flexible joints with various lengths in the finite-element simulation and the analytical model, showing good agreement (Supplementary **Fig. 4C**). Despite the nonlinear large deformation of the elastomeric cuboid, we also show that the bending angle of the joint is almost linearly proportional to its initial length  $L$  under a constant inflation pressure  $p$  (Supplementary **Fig. 4D**).

We further study the pneumatic response of a soft finger consisting of an inner hollow cuboid elastomeric tubular structure surrounded by a network of fibers, rigid segments, and a stiff layer beneath the elastomeric tube (Supplementary **Fig. 5A**). Mimicking the dimensions of the distal phalanx, middle phalanx, and proximal phalanx in human fingers<sup>17,18</sup>, we set the total length of the finger as 85 mm and the length ratio of the top, middle, and bottom parts as 2: 3: 5 in the model (Supplementary **Fig. 5A**). We show that the ratio of the bending angles of the three joints are nearly constant due to the same pneumatic pressure applied to the three joints (Supplementary **Fig. 5B**). Moreover, the ratio of the bending angles of the three joints are independent of the total length of all flexible joints  $L_D + L_P + L_M$  as long as the ratio of the lengths of the three joints are fixed (e.g.,  $L_D:L_P:L_M = 2:4:1$ , Supplementary **Fig. 5C**).

In existing prosthetic hands<sup>1,2</sup>, the bending motion of a finger typically follows two characteristics: 1) the bending angle of  $\alpha_D$  is approximately half of that of  $\alpha_M$ ; and 2) the bending angle of  $\alpha_P$  is approximately the same as  $\alpha_M$ . Based on our analysis, we show that the central idea to mimic the motion trajectory of human fingers is to design the length ratio of the three flexible joints. Specifically, the length of the distal interphalangeal joint  $L_D$  needs to be half of the length of the metacarpophalangeal joint  $L_M$ , while the length of the proximal interphalangeal joint  $L_P$  is preferred to be the same as the length of the metacarpophalangeal joint  $L_M$ . Although we analyze the soft fingers with three flexible joints, the conclusion also applies to the thumb with two flexible joints, which will also be verified in the simulation with the finite-element model.

### **Finite-element model for the design of the soft finger**

To further verify the experimental results of the hand with five soft fingers, we develop a finite-element model of the soft fingers in ABAQUS to quantitatively predict the bending angles of the flexible joints and the motion trajectories of the fingers upon inflation. All material parameters are experimentally measured from mechanical characterizations<sup>51</sup>. The elastomeric tube is modeled as a neo-Hookean solid (Eq. 7) with the shear modulus  $\mu=85$  kPa and the ratio of bulk modulus to shear modulus  $\kappa/\mu = 1000$  to impose the near incompressibility of the material. The silicone skins on the outer surface are modeled as a linear elastic material with elastic modulus 0.125 MPa, and Poisson's ratio 0.45. The PE fibers are modeled as a linear elastic material with the Young's modulus 2.9 GPa, and Poisson's ratio 0.41. The heat-shrinkable tube is modeled as a linear elastic material with the Young's modulus 55 MPa, and Poisson's ratio 0.4. The carbon fiber-reinforced plastics is modeled as a linear elastic material with the Young's modulus 210 GPa and Poisson's ratio 0.3. The fiberglass grid is modeled as a linear elastic material with the Young's modulus 73 GPa, and Poisson's ratio 0.22.

To reduce the computational cost, we use the skin module to model the heat-shrinkable tube, the carbon fiber-reinforced plastics, and the fiberglass grid. The Ecoflex 00-30 layer are modeled as skins with uniform thickness as the outer surfaces of the fiber-reinforced inner elastomeric tube. An extra skin of a stiffer rubber material is added on the surfaces of the thumb-palm connection to model the constraint effect of the silicone layer. The elastomer of the inner tube is modeled as solid elements C3D4H. The fibers are modeled as beam elements B31. Tie constraints are set between the fibers and the elastomeric chambers of the finger actuators, the thumb actuator, and the thumb-palm connection actuator. The proximal ends of the thumb-palm connection are fixed to the rigid palm skeleton. The gravity load and a pressure load are applied to the inner surface of the tube of the soft fingers. The finite-element model is in quantitative agreement with the experimental results (Extended Data **Fig. 1**, Extended Data **Table 4** and Supplementary **Video 1**).

### **Participant recruitments**

All experiments were conducted in accordance with the declaration of Helsinki and approved by the Ethics Committee of Human and Animal Experiments of Shanghai Jiao Tong University. The transradial amputees participated in this study were recommended by Shanghai Liankang Prosthetics and Orthotics Manufacturing Co. Ltd, Shanghai, China. The amputees did not have any prior neuromuscular disorders, and were informed about the experimental procedure and signed the informed consent forms (ICFs) prior to the participation.

### **Training process for EMG decoding**

During the training process, the subject who performs the predefined grasp types (**Fig. 2H**) will be notified by the vibration from a motor placed on the socket. Each grasp type is maintained for 5 seconds and a rest period is required between two grasp types to prevent possible fatigue of the subject. In the experiments, short-time vibrations are provided at the beginning and end of each

grasp type to notify the subject to transit between different hand grasps, and a long-time vibration is provided at the end of the training session. Each channel (recorded by each EMG sensor) of the EMG signals from the subject performing a predefined grasp type is segmented into data fragments with 200-ms windows. Thereafter, a time-domain feature set from the data fragments of each channel for the predefined grasp type is extracted, including the mean absolute value, waveform length, zero-crossings, and slope sign changes. The features from different channels for the same predefined grasp type are cascaded to give a feature vector. Subsequently, the feature vectors obtained from the training data are fed into the linear discriminant analysis (LDA)<sup>40</sup> classifier (as detailed in the Supplementary Information) to specify the parameters for the predefined grasp types. The whole training session lasts about 15 min (See Extended Data **Fig. 6** and Supplementary **Video 4** for a demonstration of the training process).

Although the LDA-based surface EMG decoding algorithms can accurately classify the 5 class in laboratory settings (Supplementary **Fig. 14**), the performance will be reduced for amputees in realistic activities<sup>52</sup>. Therefore, in many demonstrations of the functions of the soft neuroprosthetic hand, we choose a single grasp classifier based on testing items of the standardized tests. We have indicated in the Video Captions either 5 class classifier or a single grasp classifier has been chosen.

### **Training process for tactile feedback**

In the training process for tactile feedback, the stimulation current is set as bi-phasic, rectangular current pulses. Based on our previous results<sup>53</sup>, we set the current amplitudes, pulse widths and frequencies for all five channels as 4 mA, 200  $\mu$ s and 20 Hz, respectively. During the training process, we compress each soft finger three times in a random order to check if the subject can discriminate the compressed finger based on the electrical stimulation. The training process lasts about 5 min.

### **Data analysis and statistics.**

All data are analyzed using the available built-in functions of MATLAB (R2016b, The Mathworks Inc., USA) and SPSS (version 22, IBM Inc., USA). All data are reported as mean values with standard deviations when indicated. In the statistical analyses of standardized tests, the factors (independent variables) are the neuroprosthetic hand type (the soft neuroprosthetic hand and the rigid neuroprosthetic hand) and task type (items J2-J7 or S1-S9). The dependent variable is the task time. All the data are demonstrated normally distributed through the Kolmogorov-Smirnov test ( $p > 0.05$ ) before significant analysis. A two-way analysis of variance (ANOVA) is used to statistically analyze the significant influences of the two factors (neuroprosthetic hand types and task types) on the task time in the two sessions (items J2-J7 or S1-S9). According to the two-way ANOVA, there is interaction between the two factors. Bonferroni correction is used to correct for multiple comparisons. Two-tailed, paired-samples  $t$ -test is used to compare the difference of blocks per minute (in the Box and Blocks Test) or words per minute (item J1) with different neuroprosthetic hand types.

## REFERENCES

1. Cordella, F. et al. Literature review on needs of upper limb prosthesis users. *Front. Neurosci.* **10** (2016).
2. Belter, J. T., Segil, J. L., Dollar, A. M. & Weir, R. F. Mechanical design and performance specifications of anthropomorphic prosthetic hands: a review. *J. Rehabil. Res. Dev.* **50**, 599 (2013).
3. Lewis, S., Russold, M. F., Diet, H. & Kaniusas, E. Satisfaction of prosthesis users with electrical hand prostheses and their suggested improvements. *Biomed. Tech.* **58**, (2013).
4. Biddiss, W. A. & Chau, T. T. Upper limb prosthesis use and abandonment: A survey of the last 25 years. *Prosthet. Orthot. Int.* **31**, 236-257 (2007).
5. Farina, D. & Aszmann, O. Bionic limbs: clinical reality and academic promises. *Sci. Transl. Med.* **6**, 257ps12 (2014).
6. Hill W. Upper limb prosthetic outcome measures (ULPOM): a working group and their findings. *JPO J. Prosthet. Orthot.* **21**, P69-P82 (2009).
7. Xu, K., Guo, W., Hua, L., Sheng, X. & Zhu, X. A prosthetic arm based on EMG pattern recognition. In *IEEE Int. Conf. on Robotics and Biomimetics (ROBIO)*. 1179-1184 (IEEE, 2016).
8. Catalano, M. G. et al. Adaptive synergies for the design and control of the Pisa/IIT SoftHand. *Int. J. Robot. Res.* **33**, 768–782 (2014).
9. Godfrey, S. B. et al. The SoftHand Pro: functional evaluation of a novel, flexible, and robust myoelectric prosthesis. *Plos One* **13**, e0205653 (2018)
10. Kanzler, C. M. et al. An Objective Functional Evaluation of Myoelectrically-Controlled Hand Prostheses: A Pilot Study Using the Virtual Peg Insertion Test. In *2019 IEEE 16th International Conference on Rehabilitation Robotics (ICORR)*. 392–397 (2019).
11. Tan, D. W. et al. A neural interface provides long-term stable natural touch perception. *Sci. Transl. Med.* **6**, 257ra138-257ra138 (2014).
12. Raspopovic, S. et al. Restoring Natural Sensory Feedback in Real-Time Bidirectional Hand Prostheses. *Sci. Transl. Med.* **6**, 222ra19-222ra19 (2014).
13. Clemente, F. et al. Non-Invasive, Temporally discrete feedback of object contact and release improves grasp control of closed-loop myoelectric transradial prostheses. *IEEE Trans. Neural Syst. Rehabil. Eng.* **24**, 1314–1322 (2016).
14. D’Anna, E. et al. A somatotopic bidirectional hand prosthesis with transcutaneous electrical nerve stimulation based sensory feedback. *Sci. Rep.* **7**, 10930 (2017).
15. Valle, G. et al. Biomimetic intraneural sensory feedback enhances sensation naturalness, tactile sensitivity, and manual dexterity in a bidirectional prosthesis. *Neuron* **100**, 37-45 (2018).
16. Osborn, L. E. et al. Prosthesis with neuromorphic multilayered e-dermis perceives touch and pain. *Sci. Robot.* **3**, eaat3818 (2018).
17. Zollo, L. et al. Restoring tactile sensations via neural interfaces for real-time force-and-slippage closed-loop control of bionic hands. *Sci. Robot.* **4**, eaau9924 (2019).
18. D’Anna, E. et al. A closed-loop hand prosthesis with simultaneous intraneural tactile and position feedback. *Sci. Robot.* **4**, eaau8892 (2019).
19. Rus, D. & Tolley, M. T. Design, fabrication and control of soft robots. *Nature.* **521**, 467–475 (2015).
20. Rich, S. I., Wood, R. J. & Majidi C. Untethered soft robotics. *Nat. Electron.* **1**, 102 (2018).
21. Polygerinos, P. et al. Soft Robotics: review of fluid-driven intrinsically soft devices; manufacturing, sensing, control, and applications in human-robot interaction. *Adv. Eng. Mater.* **19**, 1700016 (2017).
22. Hu, W., Lum, G. Z., Mastrangeli, M. & Sitti, M. Small-scale soft-bodied robot with multimodal locomotion. *Nature.* **554**, 81–85 (2018).

23. Acome, E. et al. Hydraulically amplified self-healing electrostatic actuators with muscle-like performance. *Science*. **359**, 61–65 (2018).
24. Connolly, F., Walsh, C. J. & Bertoldi, K. Automatic design of fiber-reinforced soft actuators for trajectory matching. *Proc. Natl. Acad. Sci.* **114**, 51–56 (2017).
25. Cacucciolo, V., Shintake, J., Kuwajima, Y., Maeda, S., Floreano, D. & Shea H. Stretchable pumps for soft machines. *Nature* **572**, 516-519 (2019).
26. Farrow, N. & Correll, N. A soft pneumatic actuator that can sense grasp and touch. In *IEEE Int. Conf. on Intelligent Robots and Systems (IROS)*. 2317-2323 (IEEE, 2015).
27. Ferris, D. P. & Lewis, C. L. Robotic lower limb exoskeletons using proportional myoelectric control. In *Annual Int. Conf. Proc. IEEE Eng. Med. Biol. Soc.* 2119-2124 (2009).
28. Polygerinos, P. et al. EMG controlled soft robotic glove for assistance during activities of daily living. In *IEEE Int. Conf. on Rehabilitation Robotics (ICORR)*. 55-60 (IEEE, 2015).
29. Ge, L. et al. Design, Modeling, and evaluation of fabric-based pneumatic actuators for soft wearable assistive gloves. *Soft Robot*. Doi: 10.1089/soro.2019.0105 (2020).
30. Deimel, R. & Brock O. A novel type of compliant and underactuated robotic hand for dexterous grasping. *Int. J. Robot. Res.* **35**, 161–185 (2016).
31. Scharff et al. Towards behavior design of a 3D-printed soft robotic hand. *Soft robotics: trends, applications and challenges*, Springer, 2017.
32. Zhao, H., O'Brien, K., Li, S. & Shepherd R. F. Optoelectronically innervated soft prosthetic hand via stretchable optical waveguides. *Sci. Robot.*, **1**, 7529 (2016).
33. Zhou, J. et al. BCL-13: A 13-DOF soft robotic hand for dexterous grasping and in-hand manipulation. *IEEE Robot. Autom. Lett.* **3**, 3379–3386 (2018).
34. Zhou, J. et al. A Soft-robotic approach to anthropomorphic robotic hand dexterity. *IEEE Access.* **7**, 101483-95 (2019).
35. Emerson, E. T., Krizek, T. J. & Greenwald, D. P. Anatomy, physiology, and functional restoration of the thumb. *Ann. Plast. Surg.* **36**, 180–191 (1996).
36. Gustus, A., Stillfried, G., Visser, J., Jörntell, H. & Smagt, P. Human hand modelling: kinematics, dynamics, applications. *Biol. Cybern.* **106**, 741–755 (2012).
37. Keplinger, C. et al. Stretchable, transparent, ionic conductors. *Science*. **341**, 984–987 (2013).
38. Yang, C. & Suo, Z. Hydrogel ionotronics. *Nat. Rev. Mater.* **3**, 125–142 (2018).
39. Gu, G. et al. Integrated soft ionotronic skin with stretchable and transparent hydrogel-elastomer ionic sensors for hand-motion monitoring. *Soft Robot.* **6**, 368–376 (2019).
40. Englehart, K. & Hudgins, B. A robust, real-time control scheme for multifunction myoelectric control. *IEEE Trans. Biomed. Eng.* **50**, 848–854 (2003).
41. Feix, T., Romero, J., Schmiedmayer, H., Dollar, A. M. & Kragic, D. The GRASP taxonomy of human grasp types. *IEEE Trans. Hum.-Mach. Syst.* **46**, 66–77 (2016).
42. Bullock, I. M. et al. Grasp frequency and usage in daily household and machine shop tasks. *IEEE Trans. Haptics.* **6**, 296–308 (2013).
43. Kyberd, P. J., Evans, M. & Winkel, S. An intelligent anthropomorphic hand, with Automatic Grasp. *Robotica.* **16**, 531–536 (1998).
44. Hammock, M. L., Chortos, A., Tee, B., Tok, J. & Bao Z. 25th anniversary article: The evolution of electronic skin (e-skin): a brief history, design considerations, and recent progress. *Adv. Mater.* **25**, 5997–6038 (2013).
45. Resnik, L. & Borgia, M. Reliability and validity of outcome measures for upper limb amputation. *JPO J. Prosthet. Orthot.* **24**, 192–201 (2012).

46. Phillips, S. L., Harris, M. S., Koss, L. & Latlief, G. Experiences and outcomes with powered partial hand prostheses: A case series of subjects with multiple limb amputations. *JPO J. Prosthet. Orthot.* **24**, 5 (2012).
47. Smit, G., Plettenburg, D. & Helm, F. The lightweight delft cylinder hand, the first multi-articulating hand that meets the basic user requirements. *IEEE Trans. Neural Syst. Rehabil. Eng.* **23**, 431-440 (2015).
48. Fougner, A. et al. Control of upper limb prostheses: Terminology and proportional myoelectric control- A review. *IEEE Trans. Neural Syst. Rehabil. Eng.* **20**, 663-677 (2012).
49. Hahne, J. M. et al. Simultaneous control of multiple functions of bionic hand prostheses: Performance and robustness in end users. *Sci. Robot.* **3**, eaat3630 (2018).
50. Zhuang, K. Z. et al. Shared human-robot proportional control of a dexterous myoelectric prosthesis. *Nat. Mach. Intell.* **1**, 400-411 (2019).
51. Jones, D. R. H. & Ashby, M. F. *Engineering Materials 1: An Introduction to Properties, Applications and Design* (Butterworth-Heinemann, Amsterdam; Boston, 4 edition. (2011).
52. Farina, D. et al. The extraction of neural information from the surface EMG for the control of upper-limb prostheses: emerging avenues and challenges. *IEEE Trans. Neural Syst. Rehabil. Eng.* **22**, 797-809 (2014).
53. Chai, G. et al. Characterization of evoked tactile sensation in forearm amputees with transcutaneous electrical nerve stimulation. *J. Neural Eng.* **12**, 066002 (2015).

### Data availability

The datasets generated or analyzed during the current study are available from the corresponding author on reasonable request.

**Acknowledgments:** The research was supported in part by the National Natural Science Foundation of China (grant nos. 91948302 and 51620105002), Shanghai Jiao Tong University Scientific and Technological Innovation Funds (grant no. 2019QYB08) and Massachusetts Institute of Technology. We thank the subjects for the agreements to this research. We thank M. Feng, Z. Shen and N. Ding for the participations of building the experimental setups, and Q. He for the discussions of the model and simulation. All data needed to evaluate the conclusions are presented in the paper or the supplementary materials.

### Author Contributions

G.G., N.Z., X.Y.Z and X.H.Z. conceived the idea and designed the study. X.H.Z. and G.G. proposed the decoupled design of the hand and the waist bag. G.G., N.Z. H.X., H.Y, Q.S., X.Y.Z. and X.H.Z. performed experiments and analyzed the experimental data. Y.Y., G.C., X.S. and X.Y.Z. developed the EMG sensors and electrical stimulation platform. G.G., S.L., L.G. and X.H.Z. developed the theoretical model and performed the FEM simulation for verification. X.H.Z, G.G. and X.Y.Z. directed the project. G.G., X.H.Z., N.Z., H.X. X.Y.Z. prepared the manuscript and all authors provided feedback and agree with the final version of the manuscript.

### Competing Financial Interests

G.G., N.Z., H.X., S.L. X.Y.Z., and X.H.Z. are inventors of a patent application that covers the design and fabrication of the soft neuroprosthetic hand.

## Figures and Figure Captions

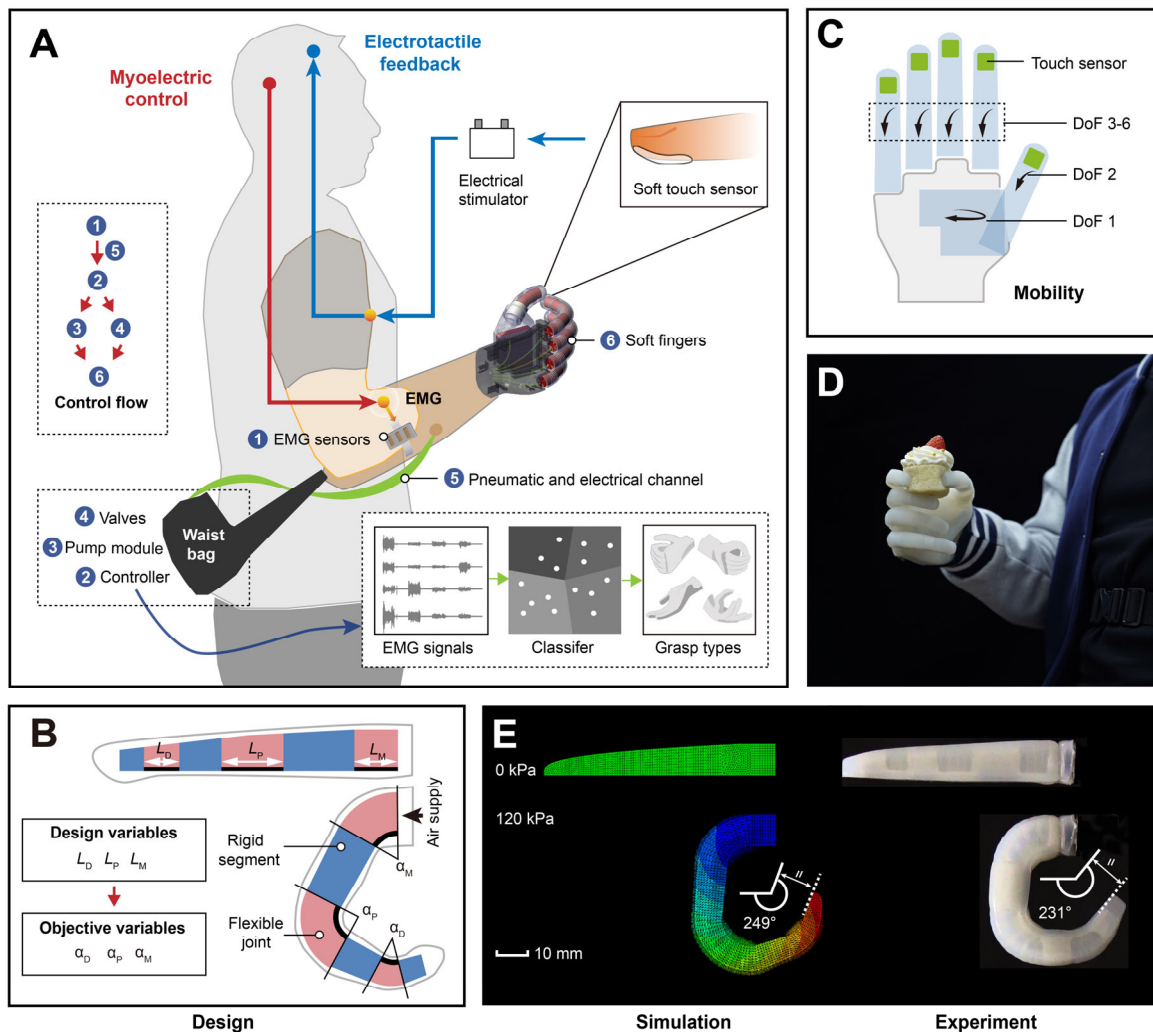


**Fig. 1 | Design and operation of the soft neuroprosthetic hand.** **A**, Schematic illustration of the soft neuroprosthetic hand mounted on a transradial amputee with a waist bag. The soft neuroprosthetic hand consists of five soft fingers and a palm, four electromyography sensors that measure the surface EMG signals of residual forearm muscles to control the hand, and five hydrogel-elastomer capacitive sensors on the fingertips that measure touch pressure and elicit electrical stimulation on the skin of the residual limb. **B**, Working principle of a soft finger made of a fiber-reinforced elastomeric tubular structure, in which three rigid segments with specific lengths are embedded to mimic the soft-joint/rigid-bone anatomy of the human finger. Our design objective is to generate the desired bending angles ( $\alpha_D$ ,  $\alpha_P$ ,  $\alpha_M$ ) of the flexible joints by tuning their lengths ( $L_D$ ,  $L_P$ ,  $L_M$ ). **C**, Schematic illustration of the soft neuroprosthetic hand with six active DoF motions and five soft capacitive touch sensors on fingertips. **D**, Photograph of a transradial amputee wearing the soft neuroprosthetic hand to grab a cupcake. **E**, Simulation of the finite-element model and experimental result of a soft finger under an applied pneumatic pressure of 120 kPa.

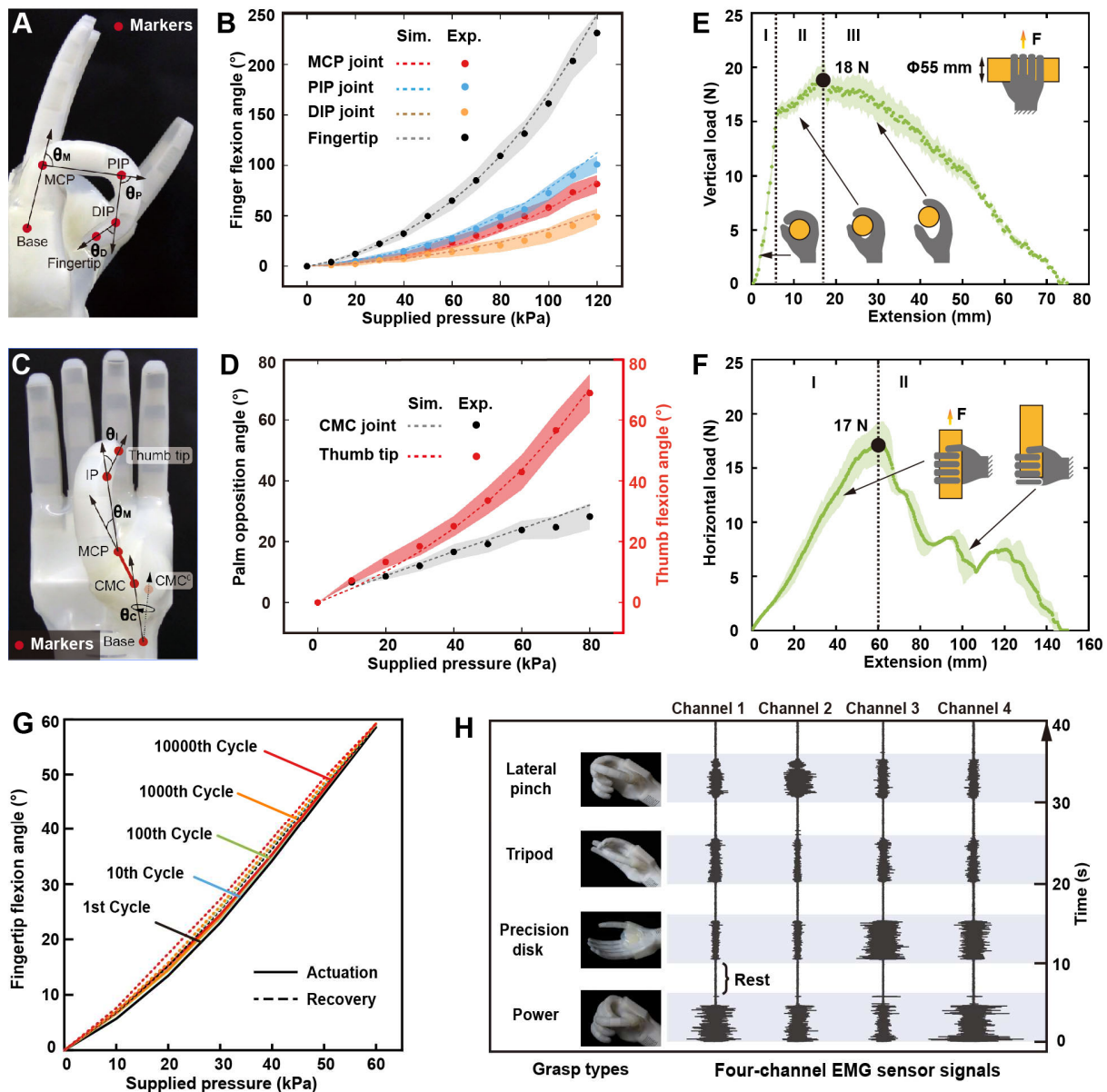


**Fig. 2 | Performance characterization of the soft neuroprosthetic hand.** A-D, Measurement and results of the ranges of motions for 1-DoF flexion fingers in (A-B), and for 2-DoF opposable thumb in (C-D). Dot markers and shaded areas represent the average and standard deviation for  $n = 3$  measurements at each data point; dash lines represent the finite-element model's predictions. Sim. and Exp. are abbreviations for simulation and experiment, respectively. MCP, PIP, DIP, CMC, and IP are abbreviations for metacarpophalangeal, proximal interphalangeal, distal interphalangeal, carpometacarpal and interphalangeal, respectively. E-F, Load capability tests of the soft neuroprosthetic hand by grasping a 55 mm-diameter cylinder at 100 kPa pneumatic pressure to the 1-DoF flexion fingers and 80 kPa pneumatic pressure to the 2-DoF thumb. G, Pressure-flexion hysteresis curves for the soft finger in the 1<sup>st</sup>, 10<sup>th</sup>, 100<sup>th</sup>, 1,000<sup>th</sup> and 10,000<sup>th</sup> cycles of actuations with the actuation frequency of 0.2 Hz. H, The four-channel EMG signals from the residual forearm muscles to decode the grasp intention (e.g., the four grasp types of Power, Precision disk, Tripod and Lateral pinch, and rest).



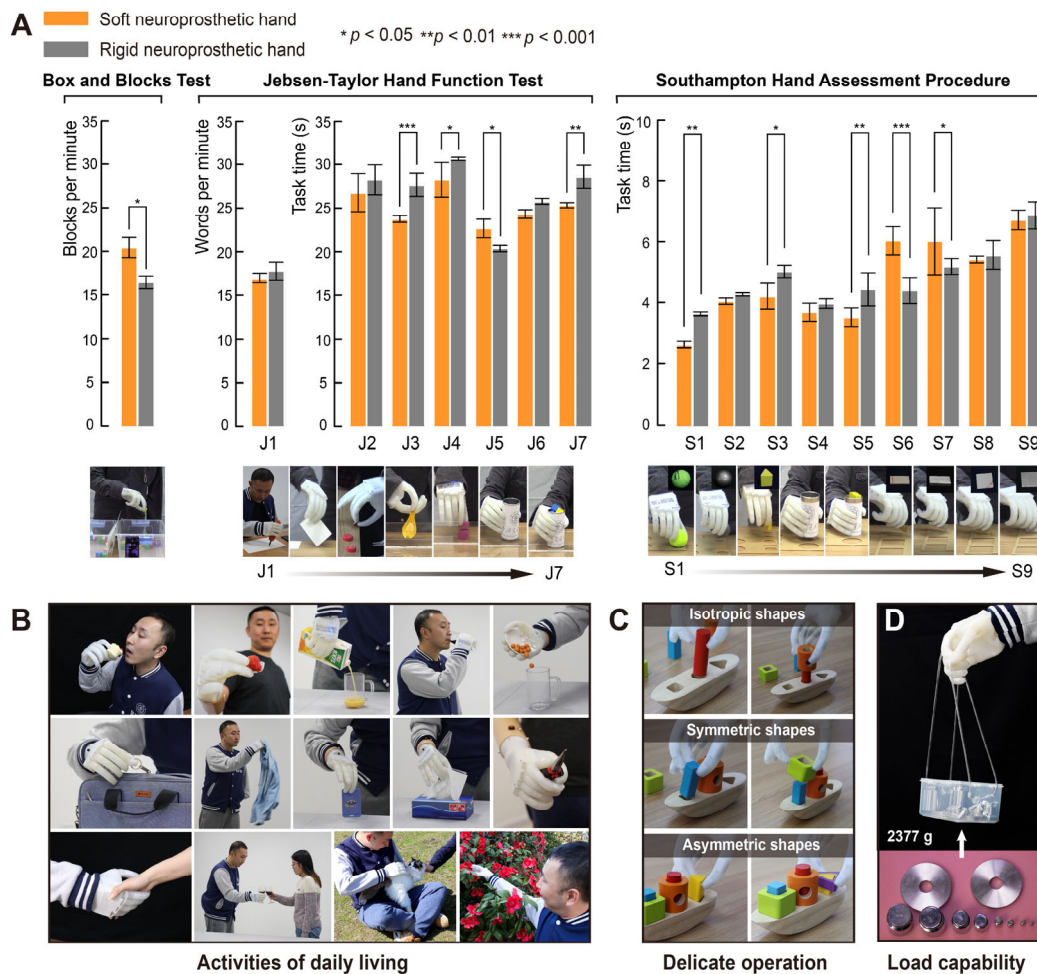


**Fig. 3 | A transradial amputee wearing the soft neuroprosthetic hand restores the versatile hand functions in daily activities. A, Evaluation of the soft neuroprosthetic hand with a set of standardized tests, including the Box and Blocks Test (e.g., counting the number of blocks per minute), all seven tasks in the Jebsen-Taylor Hand Function Test (e.g., J1: writing, J2: simulated page-turning, J3: lifting small common objects, J4: simulated feeding, J5: stacking checkers, J6: lifting large light objects, and J7: lifting large heavy objects), and nine selected tasks of the Southampton Hand Assessment Procedure (e.g., grasping nine kinds of objects, such as S1: spherical light, S2: spherical heavy, S3: tripod light, S4: power light, S5: power heavy, S6: tip light, S7: tip heavy, S8: extension light, and S9: extension heavy). Values in panel represent the mean and the standard deviation ( $n = 3$ ). A  $p$  value less than 0.05 (i.e.  $p < 0.05$ ) is considered statistically significant. B, Photographs of grasping and manipulating commonly used items in daily activities, such as food (e.g., cakes and strawberries), commodities (e.g., clothes, bags, water glasses, and tissues), and tools (e.g., pliers), and safe interaction with environment (e.g., shaking a hand, petting a cat, and touching a flower). C, Photographs of carrying out delicate tasks to handle objects with complex shapes and different sizes and then insert them in the corresponding slots precisely. D, Photograph of lifting about 2.3 kg payload (The presented image is one of three experimental trials).**

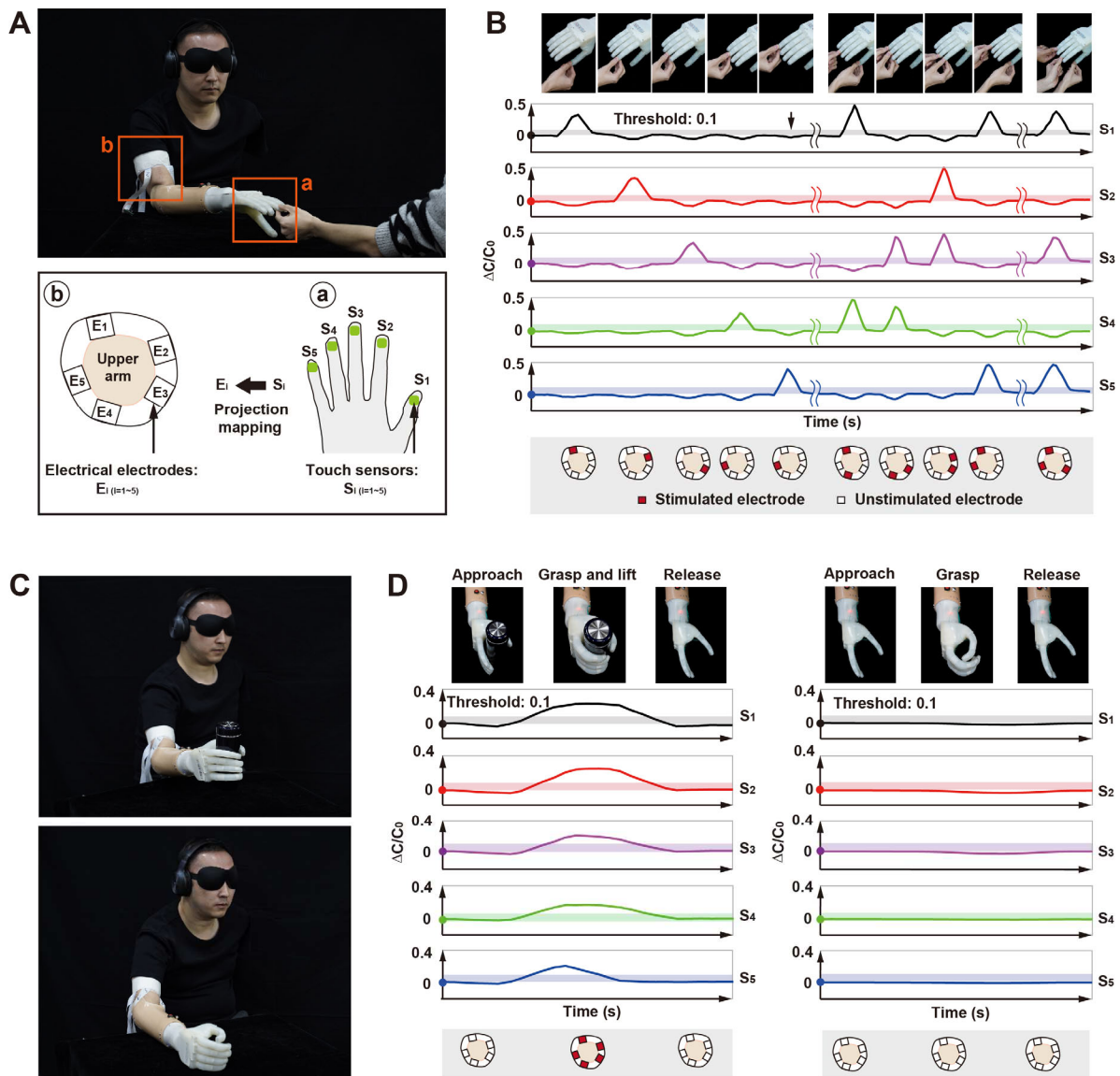
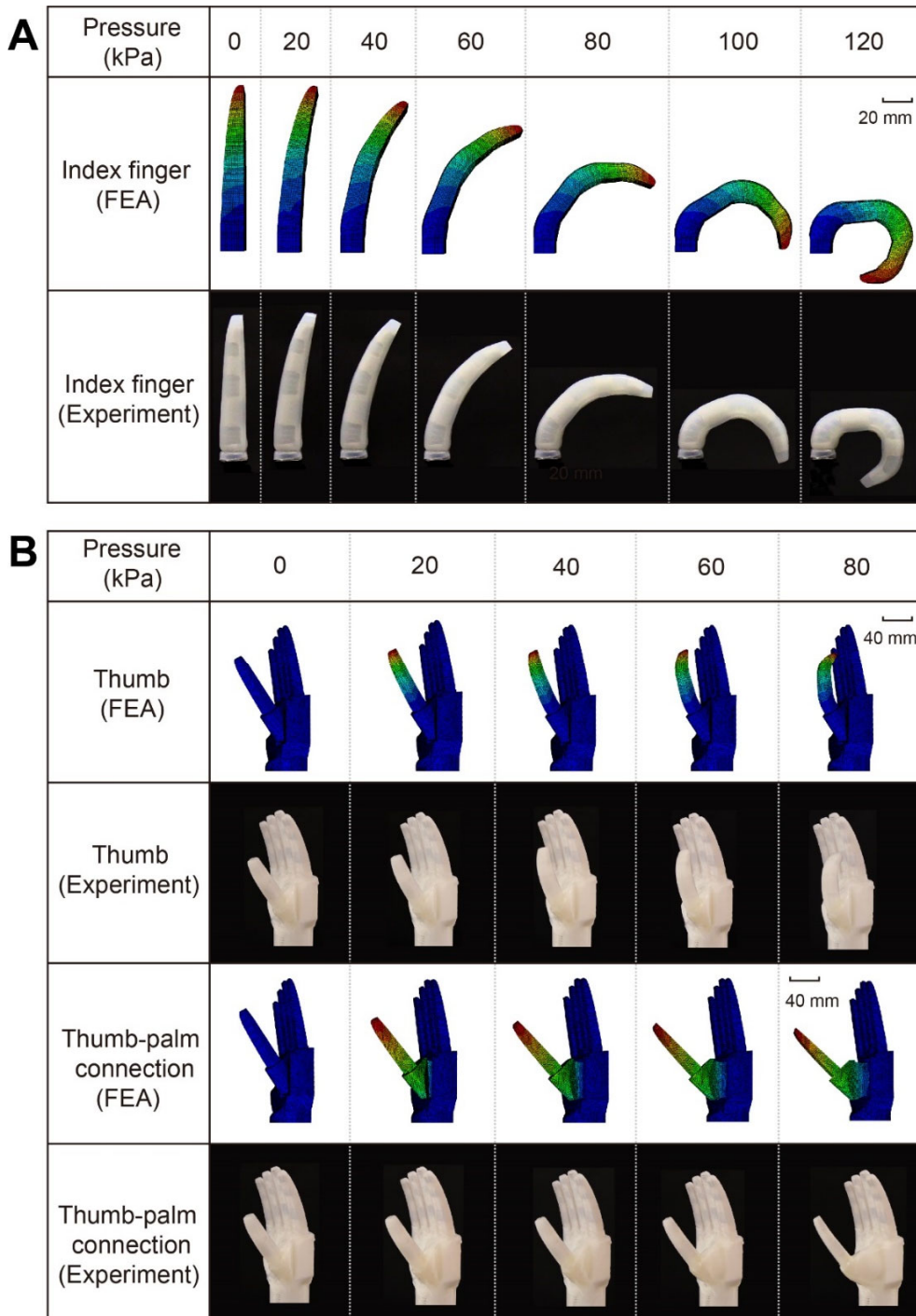
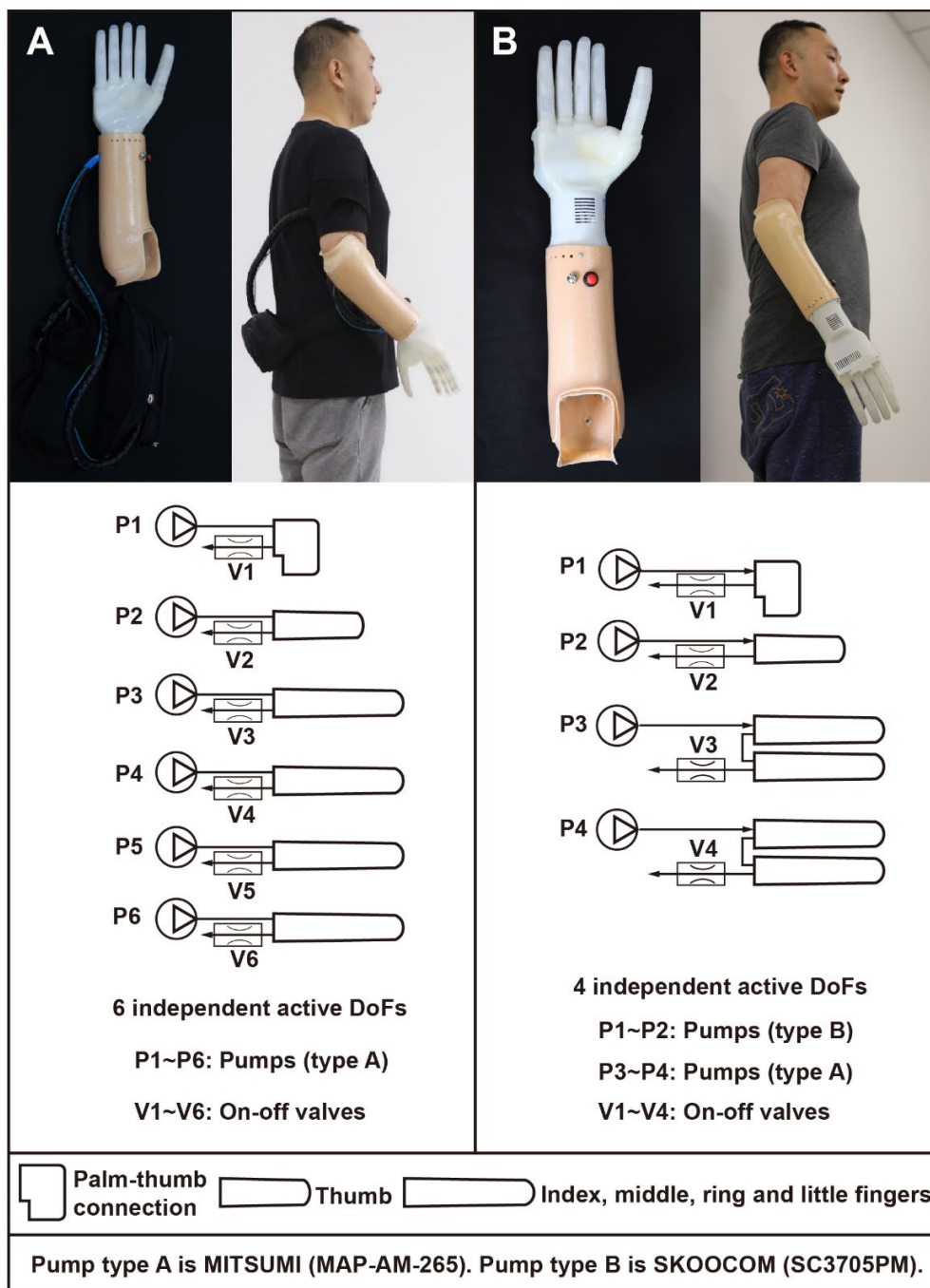


**Fig. 4 | A transradial amputee wearing the soft neuroprosthetic hand restores the primitive touch sensation and the closed-loop control in blindfolded and acoustically-shielded interaction experiments. A**, Electrical stimulation on five regions (Supplementary Fig. 9) on the residual limb of the amputee corresponding to the effective touch pressures above a threshold measured by touch sensors on five fingertips, respectively. **B**, Demonstration of the touch sensation of any individual finger or multiple fingers being compressed (the threshold  $\Delta C/C_0 = 0.1$ ). **C**, Photographs of the amputee that grasps a bottle, senses the touch pressure and lifts it up, or grasps nothing and does not lift up. **D**, Demonstration of the closed-loop control capability of the soft neuroprosthetic hand enabled by integrating the myoelectric control and tactile feedback.

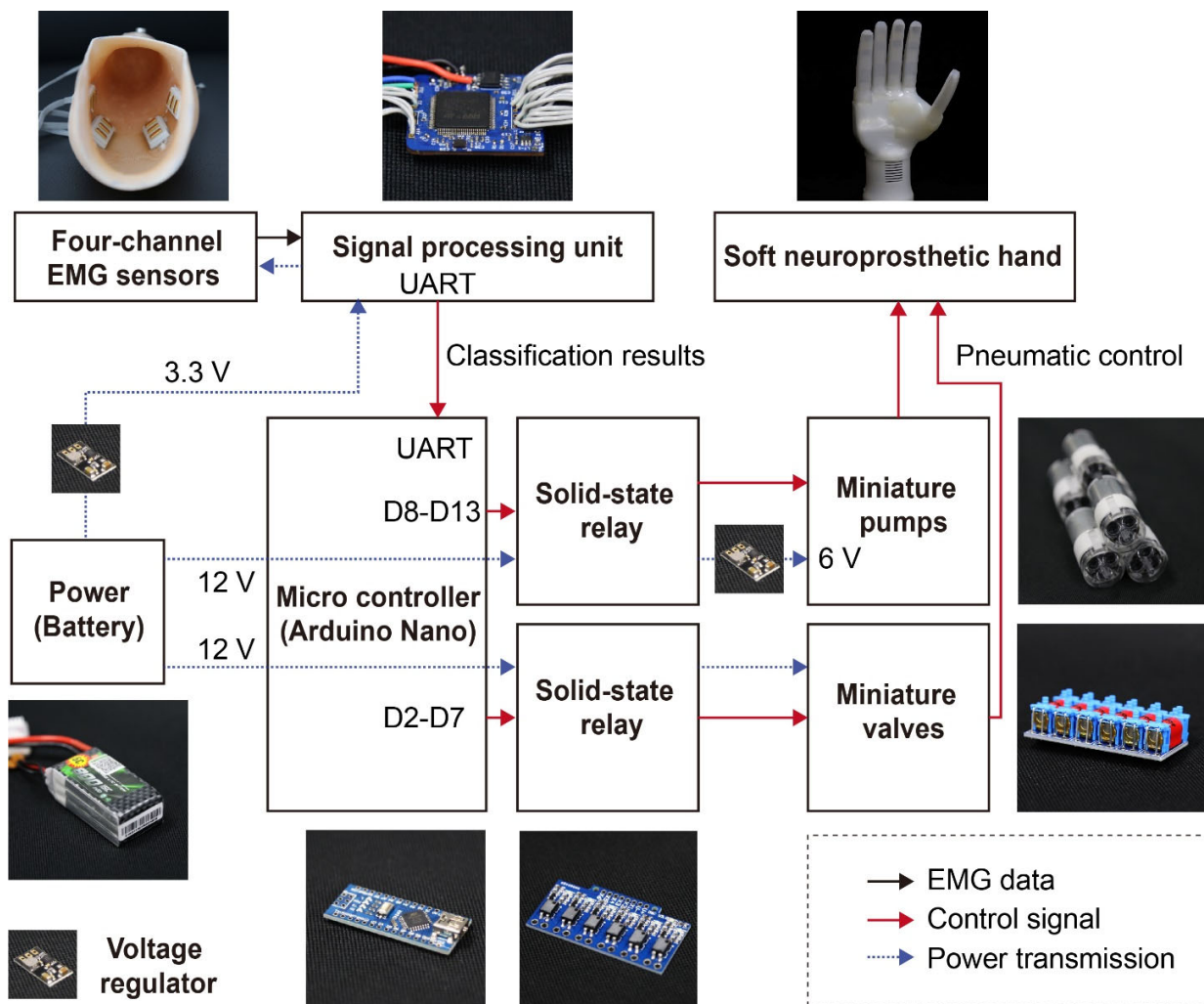
**Extended Data Figures and Tables**



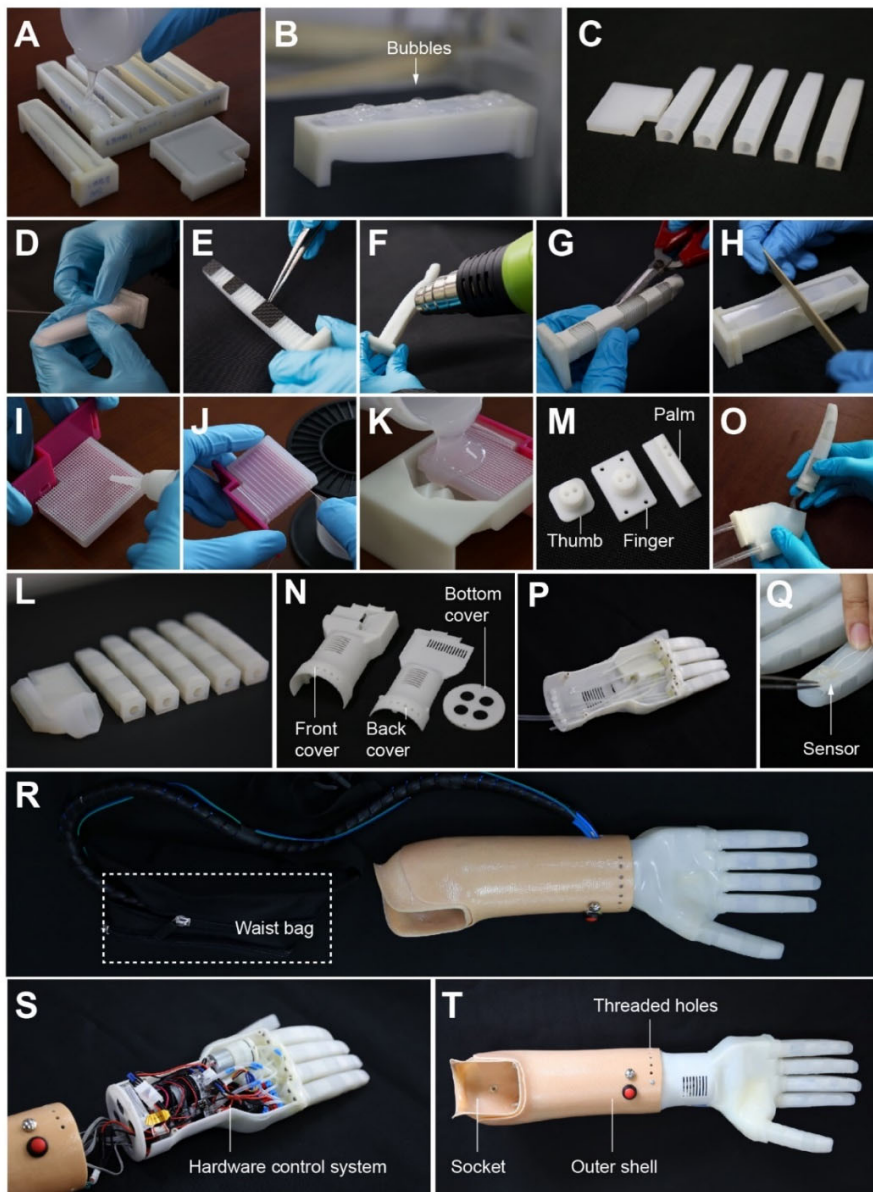
**Extended Data Fig. 1 | Simulation of the fine finite-element model and experimental results of the soft neuroprosthetic hand under different applied pneumatic pressures. A, Photographs of 1-DoF flexion of the index finger (as an exemplary motion of normal fingers) under pressures from 0 kPa to 120 kPa. B, Photographs of 2-DoF flexion of the thumb under pressures from 0 kPa to 80 kPa.**



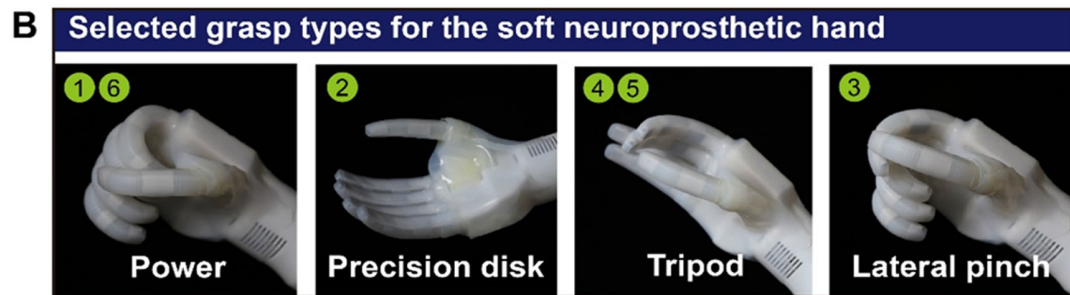
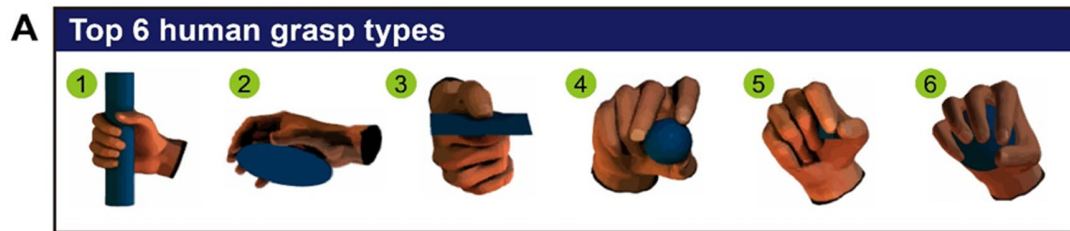
**Extended Data Fig. 2 | Schematic illustration of two kinds of soft neuroprosthetic hands and their pneumatic control schemes.** **A**, The pumps, valves, electronic boards and battery (the rechargeable lithium battery with the capacity of 800 mAh and the weight of 67 g by Geshi Inc., China) are contained in a small bag (length: 240 mm, width: 80 mm, height: 110 mm; weight: 444 g). **B**, The pumps, valves, electronic boards and battery are integrated in the palm and socket.



**Extended Data Fig. 3 | Block diagram of the myoelectric control interface in the soft neuroprosthetic hand.** The myoelectric control interface is designed for intuitive control of the soft neuroprosthetic hand. The myoelectric control is achieved by a customized onboard measurement and control system consisting of four-channel EMG sensors, control unit (including the signal processing unit for EMG decoding and the micro-controller for pneumatic actuation), pumps, valves, solid-state relays, and the power (battery and voltage regulators). The four-channel EMG sensors (embedded in the socket and mounted on the skin of residual forearm muscles) record the muscle activities of amputees, which is processed by the readout electronics with the amplification and Butterworth filtering (20-450 Hz). The signal processing unit receives the amplified and filtered signals from EMG sensors and classifies the signals into several discrete classes related to the grasp types of amputees' intention. Through a universal asynchronous receiver/transmitter (UART) port, the classification results are sent to a micro-controller (Nano, Arduino Inc., Italy). The micro-controller employs the classified grasp types to control the pumps and valves through two solid-state relays, resulting in the intuitive control of the soft neuroprosthetic hand. The pins (D2-D7) and pins (D8-D13) connect the output pins of the micro-controller relating to the corresponding pins of pump and valve relays.



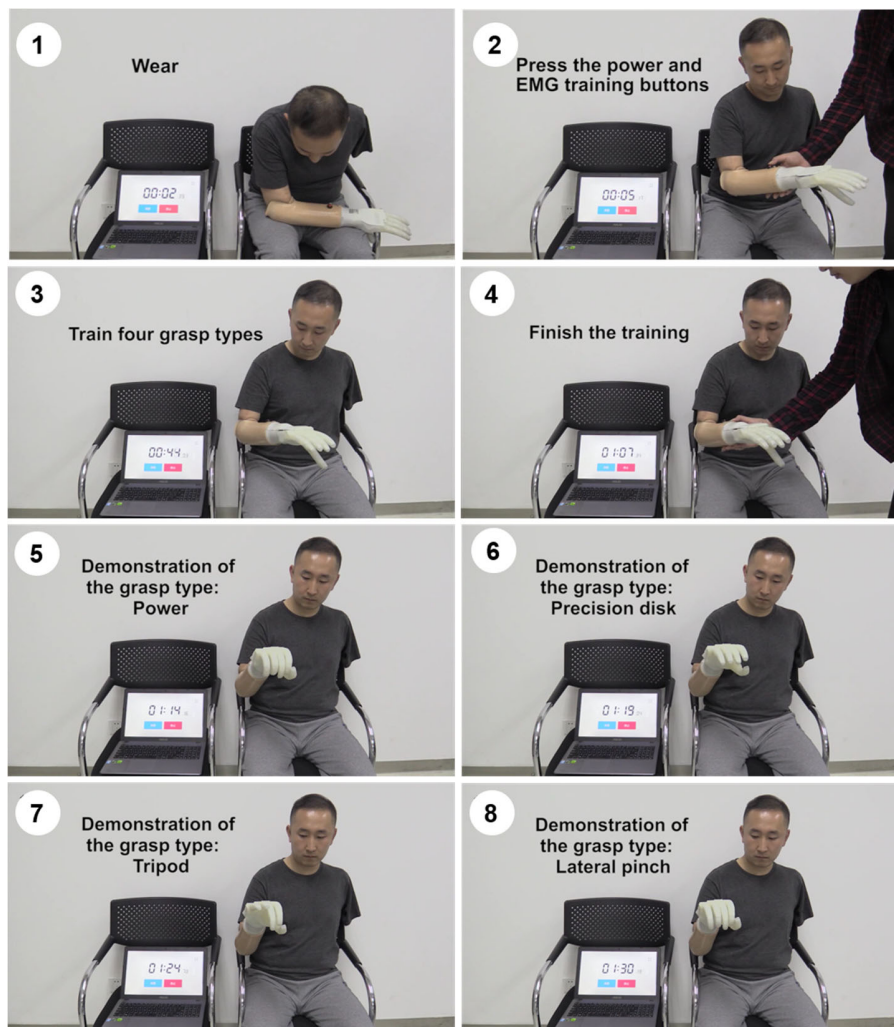
**Extended Data Fig. 4 | Fabrication and assembly of the soft neuroprosthetic hand.** **A**, Molding of inner elastomeric tubes (fingers, thumb, thumb-palm connection). **B**, Vacuum defoaming. **C**, Cured inner tubes. **D**, Winding of the finger/thumb. **E**, Carbon fiber-reinforced plastics (CFRP) laminates attachment. **F**, Sleeve wrapping. **G**, Making joint segments of the sleeve. **H**, Molding of the outer elastomeric tube of the finger/thumb. **I**, Limiting layer attachment of the thumb-palm connection. **J**, Winding of the connection pad. **K**, Molding of the outer tube of the thumb-palm connection. **L**, Cured finger/thumb, thumb-palm connection. **M**, Terminal connectors. **N**, The 3D-printed palm skeleton. **O**, Assembly of the thumb with the thumb-palm connection. **P**, Assembly of the opposable thumb and fingers to the palm skeleton. **Q**, Integrating capacitive touch sensors on the fingertips. **R**, Installing the pumps, valves, electrical boards and battery in a waist bag. **S**, Installing the pumps, valves, control boards and battery in the palm and socket. **T**, Connecting the palm skeleton with the socket to form a soft neuroprosthetic hand.



**C**

Grasp type	Power		Precision disk		Tripod		Lateral pinch	
	Flexion (°)	Pressure (kPa)	Flexion (°)	Pressure (kPa)	Flexion (°)	Pressure (kPa)	Flexion (°)	Pressure (kPa)
Palm-thumb connection	28.3	80	0	0	16.6	40	0	0
Thumb	78.8	90	23.8	60	23.8	60	78.8	90
Index finger	131.4	90	64.9	60	64.9	60	64.9	60
Middle finger	131.4	90	64.9	60	64.9	60	64.9	60
Ring finger	131.4	90	64.9	60	0	0	64.9	60
Little finger	131.4	90	64.9	60	0	0	64.9	60

**Extended Data Fig. 5 | The four EMG-controlled grasp types (excluding rest) for the soft neuroprosthetic hand and the kinematic relationship in each finger to achieve the specific grasp type. A, the six most frequently used grasp types of human hands in daily activities<sup>42</sup>. B, The regrouped four grasp types in the soft neuroprosthetic hand based on the results in (A). C, Kinematic relations of different fingers in the four predefined grasp types in (B).**



**Extended Data Fig. 6 | Still images of a subject wearing the soft neuroprosthetic hand in the training process for intuitive control.** A transradial amputee can quickly adapt to the soft neuroprosthetic hand and master its functionality by training. For the training algorithms, please refer to the Methods section. The red button is used for switching the power of the hand on/off and the silver button for switching to the training mode. As shown in the figure and supplementary **Video 4**, we can see that a subject can rapidly put on the soft neuroprosthetic hand within 3 seconds and master its function to intuitively control it after about 1 min. The training process is repeated for about 15 min.

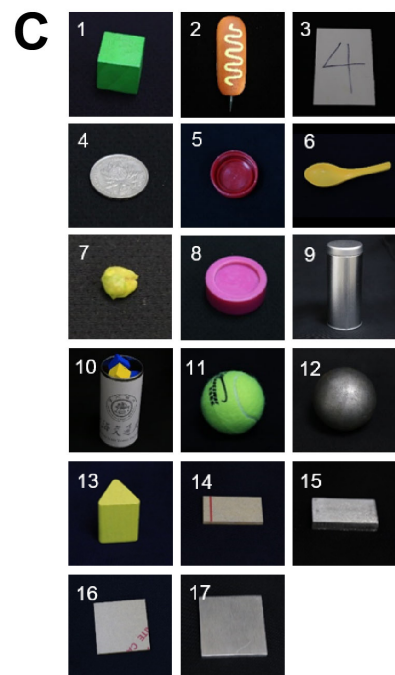


**A**

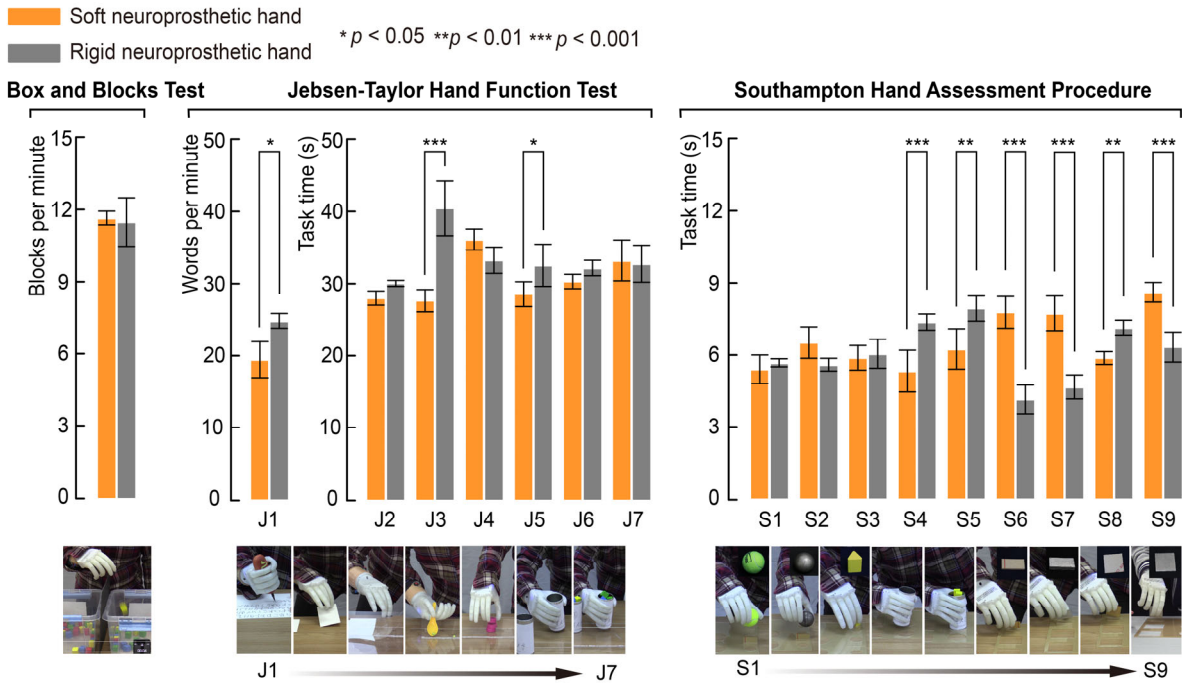
Test	Task	Task description
Box and Blocks Test	-	Counting the number of the blocks that can be grasped and transported per minute
Jebsen-Taylor Hand Function Test	J1	Writing
	J2	Simulated page-turning
	J3	Lifting small, common objects
	J4	Simulated feeding
	J5	Stacking checkers
	J6	Lifting large, light objects
	J7	Lifting large, heavy objects
Southampton Hand Assessment Procedure	S1	Spherical (light)
	S2	Spherical (heavy)
	S3	Tripod (light)
	S4	Power (light)
	S5	Power (heavy)
	S6	Tip (light)
	S7	Tip (heavy)
	S8	Extension (light)
	S9	Extension (heavy)

**B**

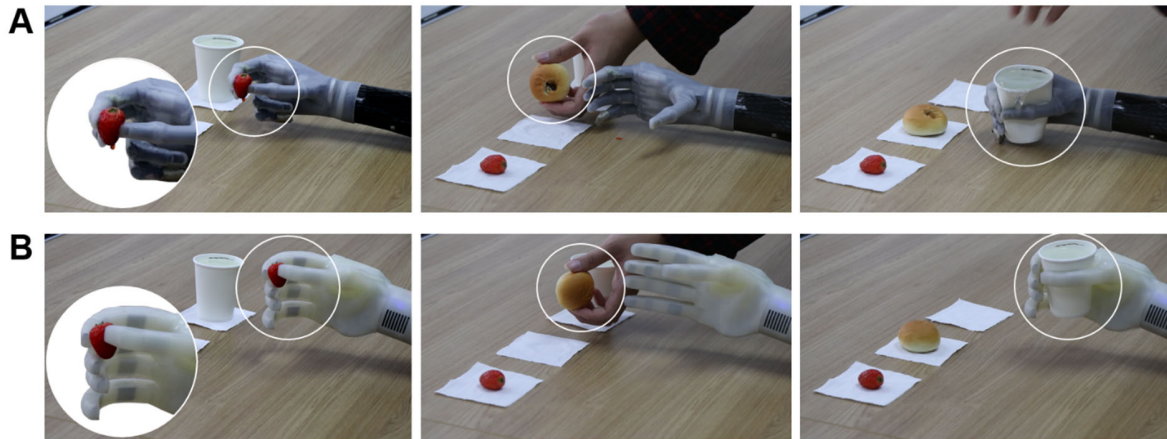
No.	Task involved	Object	Weight (g)	Dimension (mm×mm×mm)
1	BBT	Woodblock	9.7	25×25×25
2	J1	Mark pen	36.2	20×10×100
3	J2	Paper card	6.4	12.5×7.5×1
4	J3	Coin	6.1	25×25×2
5	J3	Bottle cap	1.6	32×32×12
6	J4	Spoon	14.6	127×42×48
7	J4	Pea	0.3	11×10×7
8	J5	Checker	17.1	40×40×15
9	J6, S4	Empty bottle	92.5	67×67×145
10	J7, S5	Full bottle	191.7	67×67×145
11	S1	Sphere object (light)	57.6	63×63×63
12	S2	Sphere object (heavy)	234.5	60×60×60
13	S3	Tripod object (light)	12.3	30×31×40
14	S6	Tip object (light)	7.1	50×25×5
15	S7	Tip object (heavy)	88.4	50×25×5
16	S8	Extension object (light)	14.1	50×50×5
17	S9	Extension object (heavy)	176.2	50×50×5



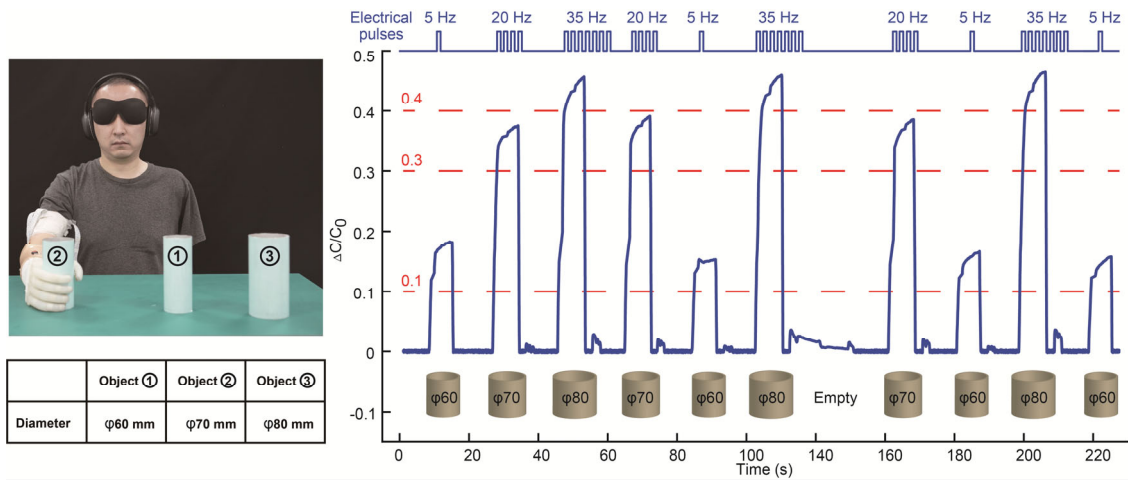
**Extended Data Fig. 7 | Descriptions of the standardized tests to evaluate the function of the soft neuroprosthetic hand. A,** Testing tasks, including the Box and Blocks Test (BBT), all seven tasks in the Jebsen-Taylor Hand Function Test (i.e., J1-J7), and nine selected tasks in the Southampton Hand Assessment Procedure (i.e., S1-S9). **B and C,** Weights, dimensions and still images of the 17 objects used in the standardized tests.



**Extended Data Fig. 8 | Evaluation of the soft neuroprosthetic hand on another transradial amputee with the standardized tests (the same as in Fig. 3A), including the Box and Blocks Test (e.g., counting the number of blocks per minute), all seven tasks in the Jebsen-Taylor Hand Function Test (e.g., J1-writing, J2-simulated page-turning, J3-lifting small common objects, J4-simulated feeding, J5-stacking checkers, J6-lifting large light objects, and J7-lifting large heavy objects), and nine abstract tasks of the Southampton Hand Assessment Procedure (e.g., grasping nine kinds of objects, such as S1-spherical light, S2-spherical heavy, S3-tripod light, S4-power light, S5-power heavy, S6-tip light, S7-tip heavy, S8-extension light, and S9-extension heavy). Values in panel represent the mean and the standard deviation ( $n = 3$ ). A  $p$  value less than 0.05 ( $p < 0.05$ ) is considered statistically significant.**



**Extended Data Fig. 9 | Demonstration of the advantage of the soft neuroprosthetic hand in handling fragile objects such as a strawberry, a piece of bread and a paper cup filled with water compared to the rigid i-Limb hand. A, the soft neuroprosthetic hand. B, the i-Limb hand. Each set of tests have been performed with three experimental trials and the presented images are from one set of experiments (Supplementary Video 7).**



**Extended Data Fig. 10 | Experimental setup and results of the subject wearing the soft neuroprosthetic hand to discriminate three cylinders with different diameters.** In this test, we program the stimulation frequencies of the electrical pulses based on the different ranges of  $\Delta C/C_0$  of the touch sensor on the middle finger (i.e., no stimulation when  $\Delta C/C_0 \leq 0.1$ , 5 Hz when  $0.1 < \Delta C/C_0 \leq 0.3$ , 20 Hz when  $0.3 < \Delta C/C_0 \leq 0.4$ , and 35 Hz when  $\Delta C/C_0 > 0.4$ ). The statistical results demonstrate that the subject can correctly discriminate the grasped subject with an accuracy of 96.25% (77 successes in all 80 tests).

**Extended Data Table 1 | Comparison of the soft neuroprosthetic hand with reported soft hands mainly composed of elastomers.**

Soft hands	Finger structure	Joint number of each finger	Tactile Sensor	EMG Sensor	Applications on amputees
Deimel et al., 2016 <sup>30</sup>	Fiber reinforced elastomers	1	No	No	No
Scharff et al., 2016 <sup>31</sup>	Bellow-type elastomers	1	No	No	No
Zhao et al., 2016 <sup>32</sup>	Fiber reinforced elastomers	1	Optoelectronic strain sensors	No	No
Wall et al., 2017 <sup>33</sup>	Fiber reinforced elastomers	1	Liquid metal strain sensors and pressure sensor	No	No
Zhou et al., 2018 <sup>34</sup>	Fiber reinforced elastomers	3	No	No	No
Zhou et al., 2019 <sup>35</sup>	Fiber reinforced elastomers	3	No	No	No
Festo Inc., 2019*	Bellow-type elastomers with textile knitted fabric	3	Inertial sensors and tactile force sensors	No	No
<b>This work</b>	<b>Fiber reinforced elastomers embedded with rigid segments</b>	<b>3</b>	<b>Ionic hydrogel elastomer touch sensors</b>	<b>Yes</b>	<b>Yes</b>






**Note:** \*see the website (<https://www.festo.com/group/en/cms/13508.htm>) for detailed information.

**Extended Data Table 2 | Detailed information of the mechanical components and electrical components of the soft neuroprosthetic hand.**

Component	Dimension (mm <sup>3</sup> )	Weight (g)	Materials and parameters of each component	Price (USD)
<b>Soft neuroprosthetic hand (total weight of 292 g)</b>				
<b>Thumb</b>	100×24×20	26	Dragonskin 10 for inner elastomeric tube. Ecoflex 0030 for outer elastomeric tube. CFRP plates from TORAY (3K), Polyethylene thread from Yunshangpiao Co. Ltd are attached to the inner tube.	~3
<b>Index, middle, ring, and little fingers</b>	110×24×20 (per piece)	112 (4 pieces)		~12
<b>Thumb-palm connection</b>	75×50×20	41	Dragonskin 10 for inner elastomeric tube. Ecoflex 0030 for outer elastomeric tube. Polyethylene thread from Yunshangpiao Co. Ltd are attached to the inner tube.	~3
<b>Palm with skin</b>	94×78×132	110	Palm skeleton is 3d printed with Imagine 8000 (SOMOS). Skin is fabricated with Ecoflex 0030.	~22
<b>Hydrogel-elastomer sensors</b>	13×13×1.9	3 (5 pieces)	Material: pAAm ionic hydrogel and dielectric elastomer. Linearity: ~0.94 and sensitivity: ~0.016 kPa <sup>-1</sup> .	~5
<b>Hardware of pneumatic control systems in a waist bag (total weight of 444 g)</b>				
<b>Pneumatic Control unit</b>	45×18×7.2	5	Arduino (Nano). 5-12 V, 12-channel input/output pins	~22
<b>Pump</b>	67×27×27	312 (6 pieces)	MITSUMI (MAP-AM-265). Maximum pressure: 90 kPa; Flow rate: 2.0 LPM; Voltage: 6 V; Noise: 55 dB	~30
<b>Valve</b>	23×12×8	30 (6 pieces)	Parker (X-valve) 2-way normal closed, directional; Voltage: 12 V	~210
<b>Relay</b>	54×30×5	14 (2 pieces)	Customized. Voltage: 12 V; 6 channels	~20
<b>Voltage regulator</b>	18×10×2.6	6 (6 pieces)	Customized. Input voltage range: 4-36 V	~6
<b>Battery</b>	57×29×22	67	Geshi. Capacity: 800 mAh; Voltage: 11.1 V (~12 V)	~10
<b>Signal processing unit for EMG sensors</b>	30×30×8	10	Customized. Voltage: 3.3 V; A/D: 12 bit. Bandpass filter: 20-450 Hz	~22
<b>Customized socket (total weight of 375.5 g)</b>				
<b>Body of the socket</b>	274×95×90	335.5	Customized	
<b>EMG sensors</b>	35×22×10	40 (4 pieces)	Customized. Material: gold-plated copper	~100
<b>Appendants</b>				
Pneumatic tube (PUN-H-3x0.5) from Festo Co. Ltd and electrical wire from ZUOYOU ZHONGGONG company.				~3

**Extended Data Table 3 | Comparison of the soft neuroprosthetic hand with representative commercially-available neuroprosthetic hands. (A) Comparison of the weight. (B) Comparison of the actuation mechanism, active DoFs, the number of joints, and bending angles of the joints.**

**A**

Prosthetic hands and company	Our work	i-Limb by Touch Bionics	Bebionic by RSL Steeper	Vincent by Vincent Systems	Michelangelo by Ottobock
Image					
Weight (g)	292	628	588	NP	420
Size (mm×mm)	190×90	182.5×85.7	188×85	180×85	196.5×120
Glove skin	Self-contained	Additional provided (about 76 g)	Additional provided	Additional provided	Additional provided

**B**

Prosthetic hands	Our work	i-Limb hand	Bebionic hand	Vincent hand	Michelangelo hand
Actuation method	1-6 pump(s)	6 DC motors	5 DC motors	6 DC motors	2 DC motors
Active DoFs	6	6	6	6	2
Number of joints	15	11	11	11	6
Joint coupling mechanism	Monolithic elastomers spanning all joints	Tendon linking MCP to PIP	Linkage spanning MCP to PIP	Linkage spanning MCP to PIP	Cam design with links to all fingers
MCP joints (°)	0-81	0-90	0-90	0-90	0-35
PIP joints (°)	0-100	0-90	0-90	0-100	NA
DIP joints (°)	0-49	NA	NA	NA	NA
Thumb flexion (°)	0-69	0-60	NP	NP	NP
Thumb circumduction (°)	0-28	0-95	0-68	NP	NP

**Note:** NA and NP are abbreviations for not applicable and not provided, respectively.

**Extended Data Table 4 | Relative prediction errors of the finite-element model for the 1-DoF finger and 2-DoF thumb.**

			Pressure (kPa)						
			0	20	40	60	80	100	120
1-DoF Finger	Finger MCP Joint	Exp (deg)	0	4.81	10.02	23.32	40.05	58.06	81.37
		Sim (deg)	0	3.66	10.16	20.16	35.34	57.09	84.02
		Relative error	0%	23.96%	1.43%	13.55%	11.76%	1.67%	3.25%
	Finger PIP Joint	Exp (deg)	0	5	14.74	27.29	48.75	72.62	100.88
		Sim (deg)	0	5.82	15.74	29.97	49.94	77.28	112.58
		Relative error	0%	16.38%	6.76%	9.83%	2.44%	6.41%	11.60%
	Finger DIP joint	Exp (deg)	0	2.33	7.55	14.28	20.57	30.73	48.91
		Sim (deg)	0	2.92	7.82	14.71	24.04	36.45	52.55
		Relative error	0%	25.62%	3.61%	2.98%	16.85%	18.62%	7.44%
	Finger Tip	Exp (deg)	0	12.14	32.31	64.9	109.37	161.41	231.16
		Sim (deg)	0	12.41	33.72	64.85	109.32	170.82	249.15
		Relative error	0%	2.17%	4.37%	0.08%	0.05%	5.83%	7.78%
2-DoF Thumb	Thumb CMC Joint	Exp (deg)	0	8.58	16.61	23.79	28.26	-	-
		Sim (deg)	0	8.78	16.77	24.36	32.02	-	-
		Relative error	0%	2.32%	0.97%	2.40%	13.29%	-	-
	Thumb Tip	Exp (deg)	0	13.34	25.08	42.85	68.78	-	-
		Sim (deg)	0	10.21	24.38	43.66	70.39	-	-
		Relative error	0%	23.48%	2.81%	1.88%	2.35%	-	-

**Note:** The relative error  $e$  is calculated by  $e = \left| \frac{\theta_{\text{FEM}} - \bar{\theta}_{\text{EXP}}}{\bar{\theta}_{\text{EXP}}} \right| \times 100\%$ , where  $\theta_{\text{FEM}}$  and  $\bar{\theta}_{\text{EXP}}$  are bending angles of the finite-element model and the average experimental results ( $n = 3$ ), respectively. Sim and Exp are abbreviations for simulation and experiment, respectively.



**Extended Data Table 5 | Comparisons of the performances of the soft neuroprosthetic hand and a conventional rigid neuroprosthetic hand<sup>7</sup> on the same subject evaluated with the standardized tests. (Each item in the standardized tests is performed three times and the mean values represent the average for  $n = 3$  measurements.) Significant results ( $p < 0.05$ ) are boldface.**

	Soft neuroprosthetic hand	Rigid neuroprosthetic hand	
<b>1-Minute Box and Blocks Test</b>			
Mean number of blocks (SD)			
1-Minute Box and Blocks Test	20.3 (1.2)	16.3 (0.8)	<b>p = 0.044</b>
<b>Jebsen-Taylor Hand Function Tests</b>			
Mean number of words (SD)			
J1: Writing	16.8 (0.6)	17.7 (1.0)	p = 0.199
Mean task time (s) (SD)			
J2: Simulated page-turning	26.7 (2.2)	28.1 (1.7)	p = 0.140
J3: Lifting small, common objects	23.6 (0.4)	27.5 (1.3)	<b>p &lt; 0.001</b>
J4: Simulated feeding	28.1 (2.0)	30.5 (0.2)	<b>p = 0.023</b>
J5: Stacking checkers	22.5 (1.1)	20.2 (0.4)	<b>p = 0.026</b>
J6: Lifting large, light objects	24.2 (0.5)	25.7 (0.4)	p = 0.141
J7: Lifting large, heavy objects	25.2 (0.3)	28.5 (1.3)	<b>p = 0.003</b>
<b>Southampton Hand Assessment Procedure</b>			
Mean task time (s) (SD)			
S1: Spherical (light)	2.6 (0.1)	3.6 (0.1)	<b>p = 0.004</b>
S2: Spherical (heavy)	4.0 (0.1)	4.3 (0.1)	p = 0.499
S3: Tripod (light)	4.2 (0.4)	5.0 (0.2)	<b>p = 0.017</b>
S4: Power (light)	3.7 (0.3)	4.0 (0.2)	p = 0.410
S5: Power (heavy)	3.5 (0.3)	4.4 (0.6)	<b>p = 0.009</b>
S6: Tip (light)	6.0 (0.5)	4.4 (0.4)	<b>p &lt; 0.001</b>
S7: Tip (heavy)	6.0 (1.1)	5.2 (0.3)	<b>p = 0.018</b>
S8: Extension (light)	5.4 (0.1)	5.6 (0.5)	p = 0.675
S9: Extension (heavy)	6.7 (0.3)	6.9 (0.5)	p = 0.654

**Extended Data Table 6 | Comparisons of the performances of the soft neuroprosthetic hand and a conventional rigid neuroprosthetic hand<sup>7</sup> on another subject evaluated with the standardized tests. (Each item in the standardized tests is performed three times and the mean values represent the average for  $n = 3$  measurements.) Significant results ( $p < 0.05$ ) are boldface.**

	Soft neuroprosthetic hand	Rigid neuroprosthetic hand	
<b>1-Minute Box and Blocks Test</b>			
	Mean number of blocks (SD)		
1-Minute Box and Blocks Test	11.7 (0.3)	11.5 (1.0)	$p = 0.808$
<b>Jebsen-Taylor Hand Function Tests</b>			
	Mean number of words (SD)		
J1: Writing	19.5 (2.5)	24.8 (1.0)	$p = 0.026$
	Mean task time (s) (SD)		
J2: Simulated page-turning	28.0 (1.0)	30.1 (0.4)	$p = 0.231$
J3: Lifting small, common objects	27.7 (1.5)	40.5 (3.7)	$p < 0.001$
J4: Simulated feeding	36.2 (1.4)	33.3 (1.8)	$p = 0.104$
J5: Stacking checkers	28.6 (1.7)	32.6 (2.9)	$p = 0.027$
J6: Lifting large, light objects	30.4 (1.0)	32.2 (1.1)	$p = 0.283$
J7: Lifting large, heavy objects	33.3 (2.8)	32.8 (2.6)	$p = 0.786$
<b>Southampton Hand Assessment Procedure</b>			
	Mean task time (s) (SD)		
S1: Spherical (light)	5.4 (0.6)	5.7 (0.2)	$p = 0.572$
S2: Spherical (heavy)	6.5 (0.7)	5.6 (0.3)	$p = 0.052$
S3: Tripod (light)	5.9 (0.5)	6.1 (0.6)	$p = 0.717$
S4: Power (light)	5.3 (0.9)	7.4 (0.3)	$p < 0.001$
S5: Power (heavy)	6.2 (0.8)	7.9 (0.5)	$p = 0.001$
S6: Tip (light)	7.8 (0.7)	4.2 (0.6)	$p < 0.001$
S7: Tip (heavy)	7.7 (0.7)	4.7 (0.5)	$p < 0.001$
S8: Extension (light)	5.9 (0.3)	7.1 (0.3)	$p = 0.009$
S9: Extension (heavy)	8.6 (0.4)	6.3 (0.6)	$p < 0.001$

## **Description of Supplementary Videos in Supplementary Information**

### **Supplementary Video 1:**

Simulation and experiments of individual motion of five soft fingers.

### **Supplementary Video 2:**

Demonstration of independent control of six DoFs with one pump.

### **Supplementary Video 3:**

Demonstration of the durability of a soft finger.

### **Supplementary Video 4:**

Demonstration of fast wearing and training of a soft neuroprosthetic hand. In this video, the EMG decoder uses a five class classifier for all the four grasps (Power, Precision disk, Tripod and Lateral pinch) and rest type.

### **Supplementary Video 5:**

Evaluation of the soft neuroprosthetic hand with the standardized tests. In this video, the EMG decoder uses a two class classifier for the single grasp type and rest type according to different items of the standardized tests (For a fair comparison, the EMG decoder is same for the rigid neuroprosthetic hand as shown in Supplementary Video 6). Specifically, the “Power” grasp type is used for the items J1, J6, J7, S1, S2, S4 and S5; the “Precision disk” grasp type is used for the items J2, S8 and S9; the “Tripod” grasp type is used for the Box and Blocks Test, items J3, J5, S3, S6 and S7; the “Lateral pinch” grasp type is used for the item J4.

### **Supplementary Video 6:**

Experimental results of the standardized tests by the same subject wearing a rigid neuroprosthetic hand. In this video, the EMG decoder uses a two class classifier for the single grasp type and rest type according to the different items of the standardized tests (For a fair comparison, the EMG decoder is same for the soft neuroprosthetic hand as shown in Supplementary Video 5). Specifically, the “Power” grasp type is used for the items J1, J6, J7, S1, S2, S4 and S5; the “Precision disk” grasp type is used for the items J2, S8 and S9; the “Tripod” grasp type is used for the Box and Blocks Test, items J3, J5, S3, S6 and S7; and the “Lateral pinch” grasp type is used for the item J4.

### **Supplementary Video 7:**

Demonstration of the compliant advantage of the soft neuroprosthetic hand. A subject wearing the soft neuroprosthetic hand and a rigid i-Limb hand to grasp fragile objects (e.g., strawberry, bread, paper cup). The rigid neuroprosthetic hand damages the strawberry and bread, and tends to crush the paper cup. In this video, the EMG decoder uses a two class classifier for the “Precision disk” grasp type and rest type.

### **Supplementary Video 8:**

Demonstration of the four EMG-controlled grasp types. In this video, the EMG decoder uses a five class classifier for all the four grasps (Power, Precision disk, Tripod and Lateral pinch) and rest type.

### **Supplementary Video 9:**

Demonstration of versatile hand functions in daily activities of the subject. In this video, the EMG decoder uses a two class classifier for the single grasp type and rest type according to different tasks in daily activities. Specifically, the “Power” grasp type is used for handling water glasses, paper drinks and clothes; the “Precision disk” grasp type is used for shaking hands, petting a cat, handling

cakes and dishes; the “Tripod” grasp type is used for gripping cards and chips; and the “Lateral pinch” grasp type is used for zippering up the bag.

**Supplementary Video 10:**

Demonstration of handling objects with different shapes and sizes. A subject can successfully carry out delicate tasks to handle objects with complex shapes and different sizes and then insert them in the corresponding slots precisely. In this video, the EMG decoder uses a two class classifier for the “Tripod” grasp type and rest type.

**Supplementary Video 11:**

Demonstration of holding heavy payloads. In this video, the subject uses his own EMG signals to control the soft neuroprosthetic hand to give the “Power” grasp type for lifting a payload of 2.3 kg. The EMG decoder uses a two class classifier for the “Power” grasp type and rest type.

**Supplementary Video 12:**

Demonstration of the touch sensation of individual finger and multiple fingers. In a blindfolded and acoustically-shielded interaction experiment, an experimenter gently compressed the five fingers of the soft neuroprosthetic hand in random combinations. The subject could almost instantaneously distinguish any individual finger or multiple fingers being compressed.

**Supplementary Video 13:**

Demonstration of the closed-loop control capability of the subject. In a blindfolded and acoustically-shielded experiment, the subject uses his own EMG signals to control the soft neuroprosthetic hand to give the “Power” grasp type. If the hand firmly grasps a bottle so that the effective pressures on the five fingertips are above the threshold, the subject is informed by the electrical stimulators to lift up the bottle. In contrast, if the hand does not grasp anything that applies pressure on the fingertips, the subject does not lift up but relaxes the hand after a few seconds. The EMG decoder uses a two class classifier for the “Power” grasp type and rest type.

**Supplementary Video 14:**

Demonstration of the graded tactile feedback of the subject. In the blindfolded and acoustically-shielded experiment, the subject uses his own EMG signals to control the soft neuroprosthetic hand to give the “Power” grasp type. According to the stimulation frequencies (i.e., 5 Hz, 20 Hz or 35 Hz) of the electrical pulses, the subject can discriminate three cylinders with different diameters (i.e., 60 mm, 70 mm and 80 mm). The EMG decoder uses a two class classifier for the “Power” grasp type and rest type.

# Figures

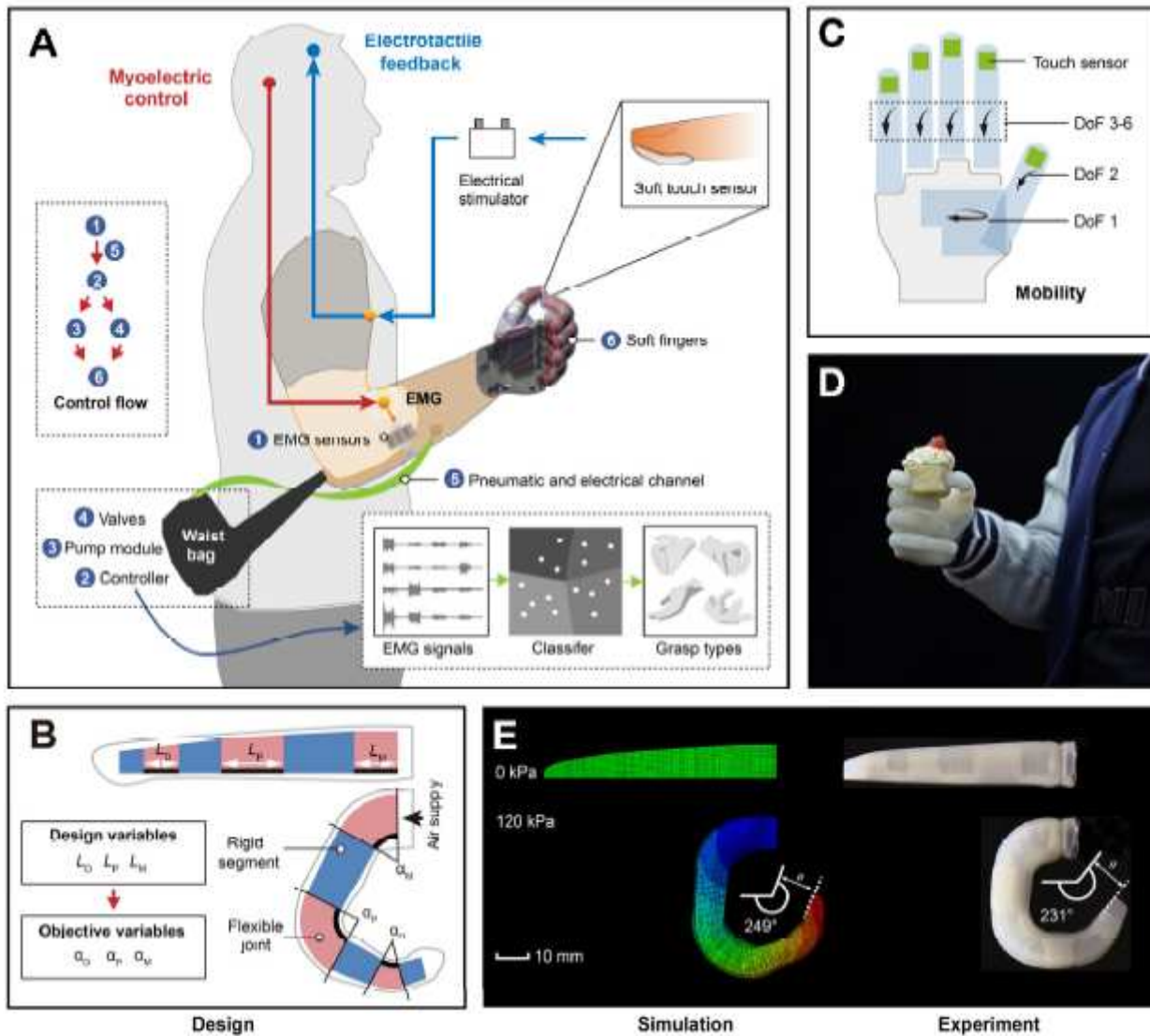


**Figure 1**

Design and operation of the soft neuroprosthetic hand. A, Schematic illustration of the soft neuroprosthetic hand mounted on a transradial amputee with a waist bag. The soft neuroprosthetic hand consists of five soft fingers and a palm, four electromyography sensors that measure the surface EMG signals of residual forearm muscles to control the hand, and five hydrogel-elastomer capacitive sensors on the fingertips that measure touch pressure and elicit electrical stimulation on the skin of the residual limb. B, Working principle of a soft finger made of a fiber-reinforced elastomeric tubular structure, in which three rigid segments with specific lengths are embedded to mimic the soft-joint/rigid-bone anatomy of the human finger. Our design objective is to generate the desired bending angles ( $\alpha_D$ ,  $\alpha_P$ ,  $\alpha_M$ ) of the flexible joints by tuning their lengths ( $L_D$ ,  $L_P$ ,  $L_M$ ). C, Schematic illustration of the soft neuroprosthetic hand with six active DoF motions and five soft capacitive touch sensors on fingertips. D, Photograph of a transradial amputee wearing the soft neuroprosthetic hand to grab a cupcake. E,

Simulation of the finite-element model and experimental result of a soft finger under an applied pneumatic pressure of 120 kPa.

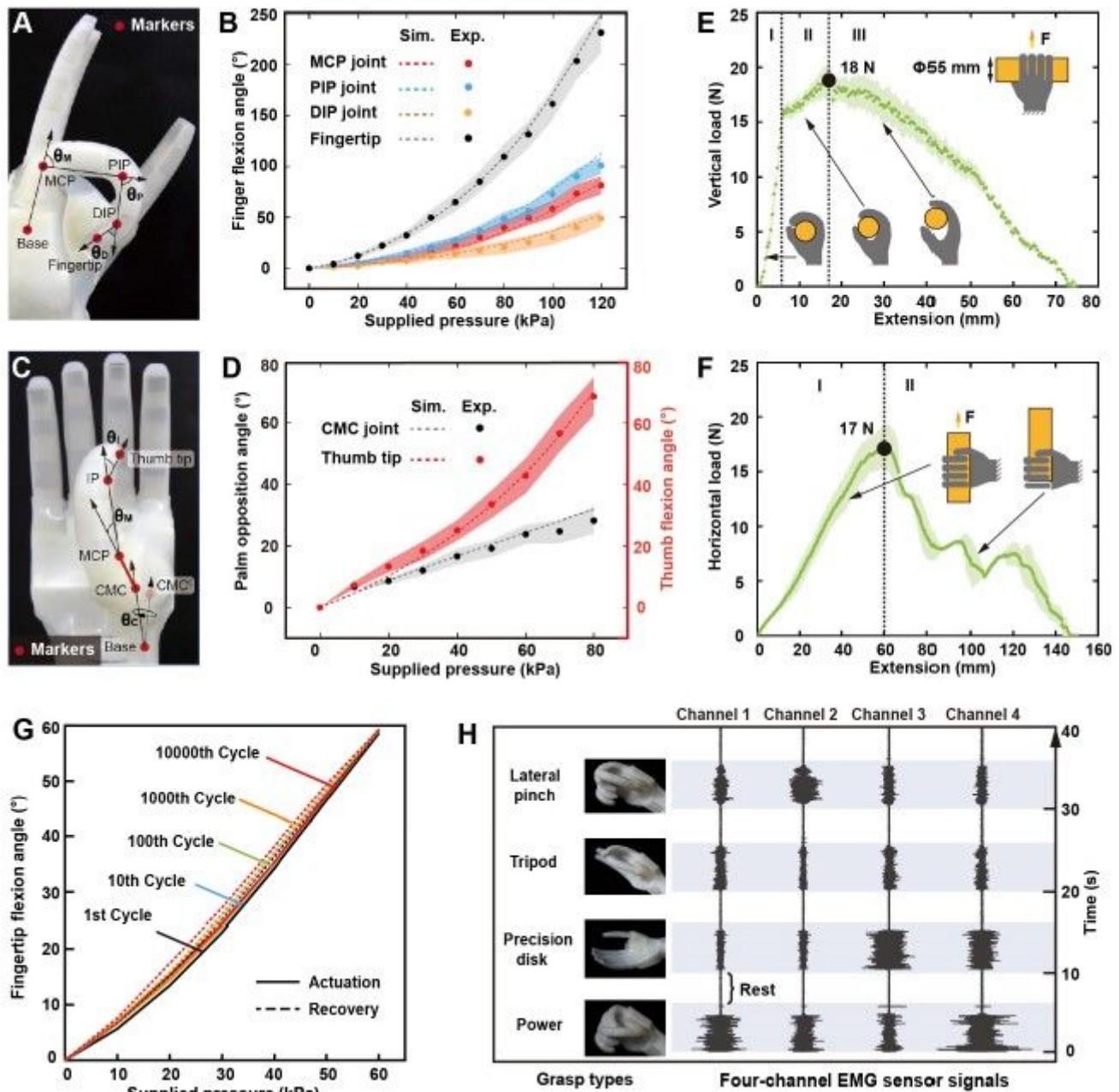
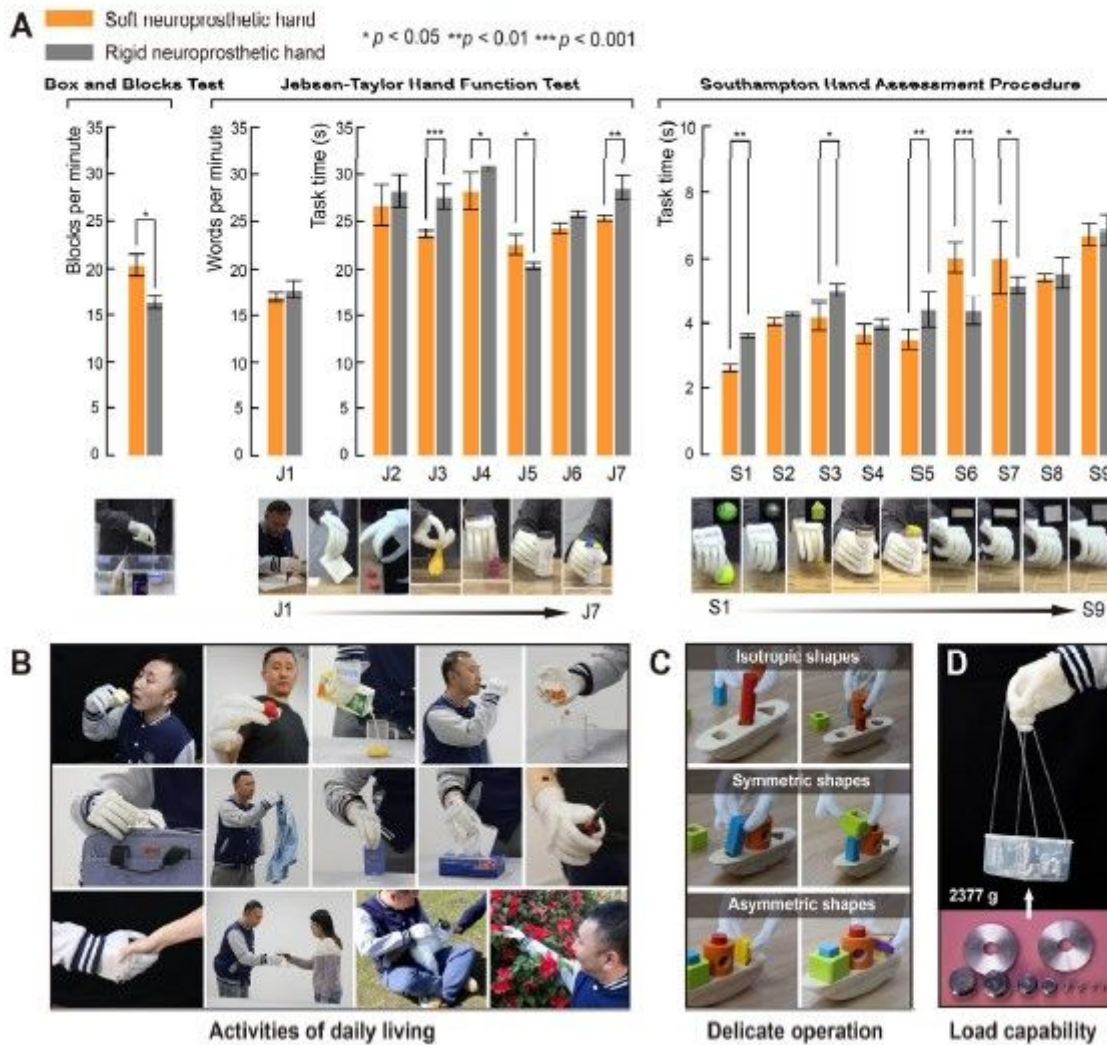


Figure 2

Performance characterization of the soft neuroprosthetic hand. A-D, Measurement and results of the ranges of motions for 1-DoF flexion fingers in (A-B), and for 2-DoF opposable thumb in (C-D). Dot markers and shaded areas represent the average and standard deviation for  $n = 3$  measurements at each data point; dash lines represent the finite-element model's predictions. Sim. and Exp. are abbreviations for simulation and experiment, respectively. MCP, PIP, DIP, CMC, and IP are abbreviations for metacarpophalangeal, proximal interphalangeal, distal interphalangeal, carpometacarpal and interphalangeal, respectively. E-F, Load capability tests of the soft neuroprosthetic hand by grasping a 55

mm-diameter cylinder at 100 kPa pneumatic pressure to the 1-DoF flexion fingers and 80 kPa pneumatic pressure to the 2-DoF thumb. G, Pressure-flexion hysteresis curves for the soft finger in the 1st, 10th, 100th, 1,000th and 10,000th cycles of actuations with the actuation frequency of 0.2 Hz. H, The four-channel EMG signals from the residual forearm muscles to decode the grasp intention (e.g., the four grasp types of Power, Precision disk, Tripod and Lateral pinch, and rest).



**Figure 3**

A transradial amputee wearing the soft neuroprosthetic hand restores the versatile hand functions in daily activities. A, Evaluation of the soft neuroprosthetic hand with a set of standardized tests, including the Box and Blocks Test (e.g., counting the number of blocks per minute), all seven tasks in the Jebsen-Taylor Hand Function Test (e.g., J1: writing, J2: simulated page-turning, J3: lifting small common objects, J4: simulated feeding, J5: stacking checkers, J6: lifting large light objects, and J7: lifting large heavy objects), and nine selected tasks of the Southampton Hand Assessment Procedure (e.g., grasping nine kinds of objects, such as S1: spherical light, S2: spherical heavy, S3: tripod light, S4: power light, S5: power heavy, S6: tip light, S7: tip heavy, S8: extension light, and S9: extension heavy). Values in panel represent the mean and the standard deviation ( $n = 3$ ). A  $p$  value less than 0.05 (i.e.  $p < 0.05$ ) is

considered statistically significant. B, Photographs of grasping and manipulating commonly used items in daily activities, such as food (e.g., cakes and strawberries), commodities (e.g., clothes, bags, water glasses, and tissues), and tools (e.g., pliers), and safe interaction with environment (e.g., shaking a hand, petting a cat, and touching a flower). C, Photographs of carrying out delicate tasks to handle objects with complex shapes and different sizes and then insert them in the corresponding slots precisely. D, Photograph of lifting about 2.3 kg payload (The presented image is one of three experimental trials).

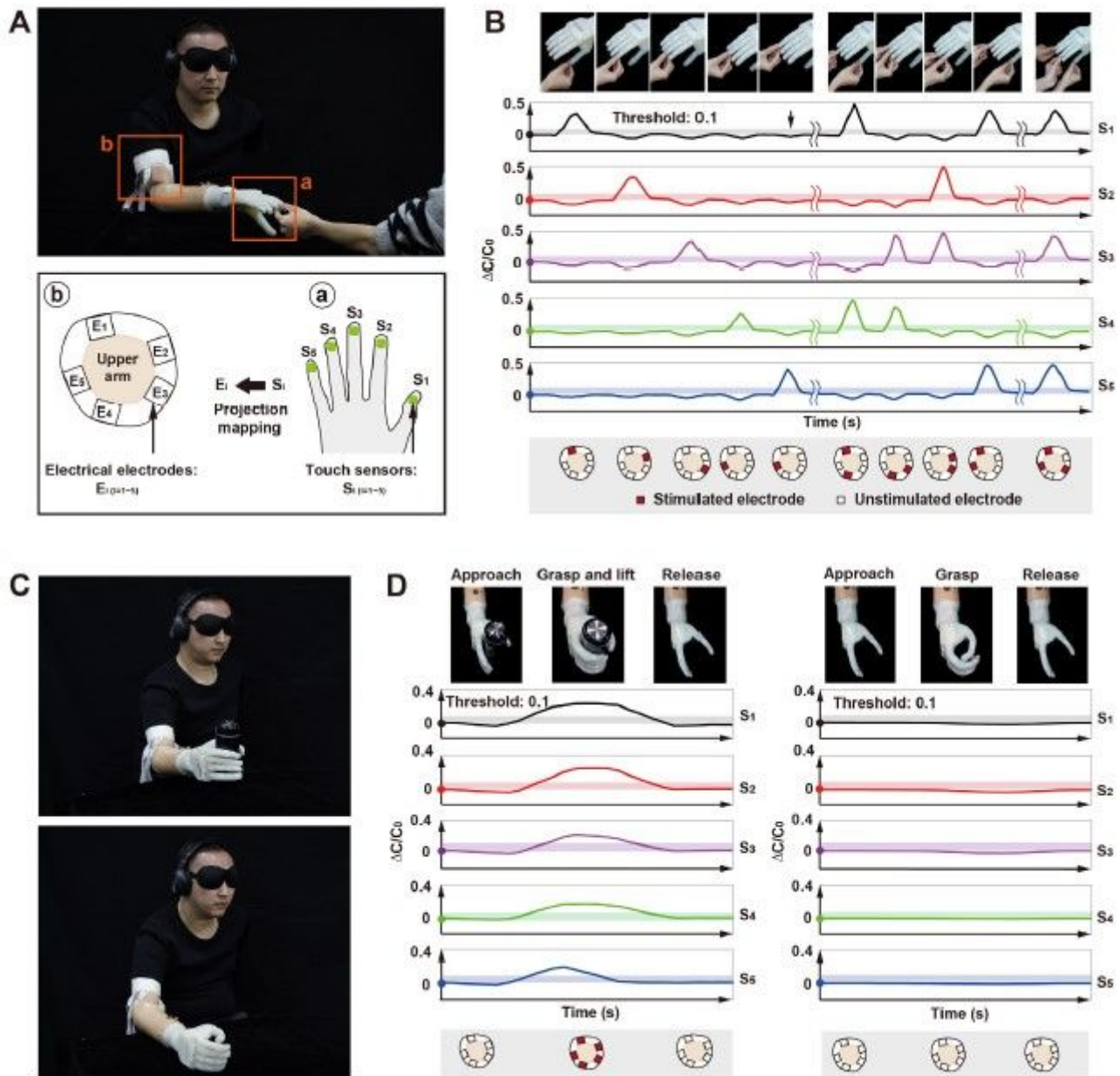


**Figure 4**

A transradial amputee wearing the soft neuroprosthetic hand restores the primitive touch sensation and the closed-loop control in blindfolded and acoustically-shielded interaction experiments. A, Electrical stimulation on five regions (Supplementary Fig. 9) on the residual limb of the amputee corresponding to the effective touch pressures above a threshold measured by touch sensors on five fingertips, respectively. B, Demonstration of the touch sensation of any individual finger or multiple fingers being



compressed (the threshold  $\Delta\mu/\mu = 0.1$ ). C, Photographs of the amputee that grasps a bottle, senses the touch pressure and lifts it up, or grasps nothing and does not lift up. D, Demonstration of the closed-loop control capability of the soft neuroprosthetic hand enabled by integrating the myoelectric control and tactile feedback.

## Supplementary Files

This is a list of supplementary files associated with this preprint. Click to download.

- [Sifornaturerevision20200721Final.pdf](#)
- [FigureS1.png](#)
- [FigureS2.jpg](#)
- [FigureS3.jpg](#)
- [FigureS4.jpg](#)
- [FigureS5.jpg](#)
- [FigureS6.png](#)
- [FigureS7.jpg](#)
- [FigureS8.jpg](#)
- [FigureS9.jpg](#)
- [FigureS10.jpg](#)
- [TableS1.png](#)
- [TableS2.png](#)
- [TableS3.png](#)
- [TableS4.png](#)
- [TableS5.png](#)
- [TableS6.png](#)
- [Supp.video1.83100video3446274qb5gpd.mp4](#)
- [Supplvideo283100video3446275qb5gpd.mp4](#)
- [Supplvideo3.83100video3446292qb5gpz.mp4](#)
- [Supplvideo4.83100video3446293qb5gp7.mp4](#)
- [Supppvideo5.83100video3446294qb5gpk.mp4](#)
- [Supplvideo6.83100video3446295qb5gpd.mp4](#)
- [Supplvideo7.83100video3446296qb5gpg.mp4](#)
- [Supplvideo8.83100video3446297qb5gp9.mp4](#)
- [Supplvideo9.83100video3446298qb5gpy.mp4](#)
- [Supplvideo10.83100video3446299qb5gp5.mp4](#)

- Supplvideo11.83100video3446300qb5gpc.mp4
- Supplvideo12.83100video3446301qb5gpf.mp4
- Supplvideo13.83100video3446302qb5gpf.mp4
- Supplvideo14.83100video3446303qb5gpf.mp4